Southern African Large Telescope
High-Resolution Spectrograph

SALT HRS

3210AE0005 Optical Design

Stuart Barnes
P.L. Cottrell
Michael D. Albrow
Graeme Kershaw
University of Canterbury

Issue 2.7
17 March 2005

Issue History

Number and file name	Person	Issue	Created	Status
3210AE0001 R4 optical.doc	SIB	1.0	27 June 2004	Created from existing docs.
		…	…	Various changes
3210AE0005 R4 optical.doc	SIB	1.9	7 July 2004	Final PDR version.
3210AE0005 SALT HRS optical	SIB	2.0	9 Feb 2005	CDR version.
	SIB	2.1	15 Feb 2005	Fibre injection details.
	SIB	2.2	1 Mar 2005	PLC comments
		2.3	6 Mar 2005	FF lamps
	MDA	2.4	8 Mar 2005	Image slicer etc
	PLC	2.5	10 Mar 2005	Edit
	SIB	2.6	13 Mar 2005	Final edit
	SIB	2.7	16 Mar 2005	Minor corrections

Table of contents

List of Figures

List of Tables

1 Scope

This document provides details of SALT HRS optical design, following the optical path.

The optical specifications for all the elements described herein are contained in 3210AD0006. The camera tests, mechanical tolerances and ghost analysis appears in 3210AA0007, a report prepared for the SALT HRS team by Prime Optics. In addition a detailed discussion of échelle theory is given in 3210AE0034. The R2 SALT HRS design Preliminary Design Review documentation contained a subset of this material.

The performance requirements of SALT HRS are described in the Functional Performance Requirements Document (3200AE0015 FPRD).

This document replaces the PDR document with the same number except that it is Issue 2.

List of referenced docs:

- 3200AE0015 FPRD
- 3200AE0018 OCDD
- 3400AE0024 FIF
- 3210AD0006 optical specification
- 3290AE0001 detector specification
- 3220AE0004 Mechanical
- 3230AE0030 Input Mechanical Design
- 3210AE0034 Optical Appendix A
- 3210AE0034 Optical Appendix B
- 3210AA0007 Optical Tolerancing

3400AE0024 Input Mechanics. The output ferrules are described in SALT HRS document 3220AE0004 Mechanical

2 SALT

The parameters of the SALT telescope are given in Table 1 and a schematic of the prime focus payload is given in Figure 1.

Table 1: SALT parameters.

Parameter	Specification
Primary mirror diameter (*D*)	11.0 m
Focal ratio	*F*/4.2
Effective focal length	46.2 m
Image scale	224 μm/arcsec
EE(80)	2.15 arcsec
EE(50)	1.29 arcsec
FWHM	1.13 arcsec

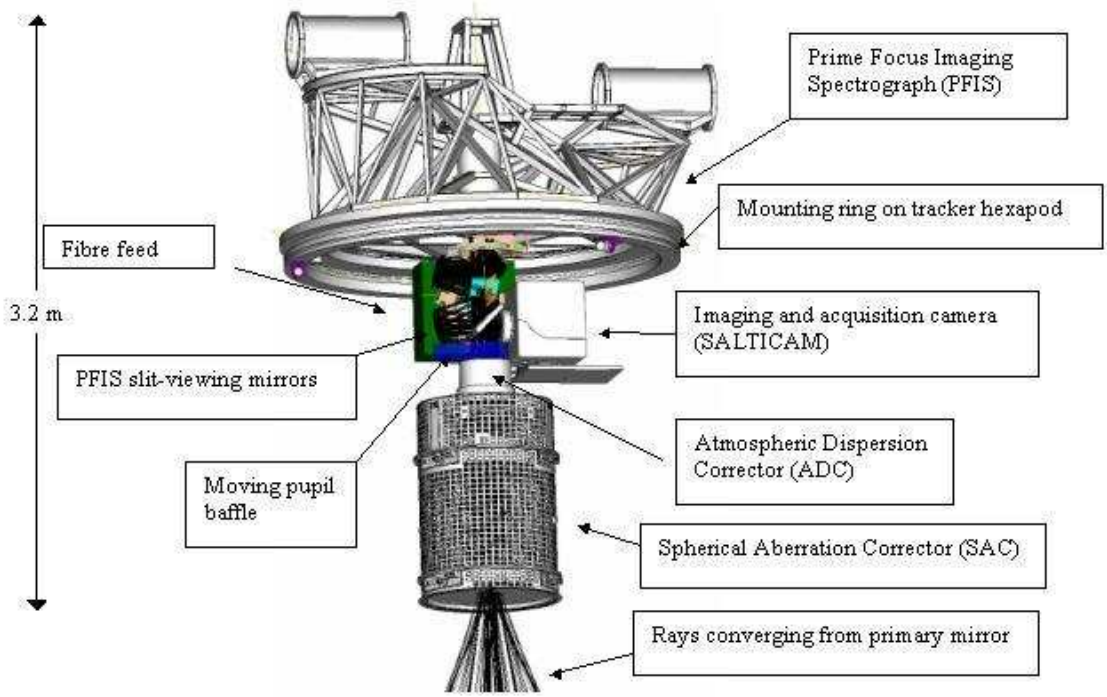

Figure 1: The SALT prime focus payload. The Fibre Instrument Feed (FIF) is located between the ADC and PFIS, alongside SALTICAM (from Buckley et al, 2004) and is fed by a removable fold mirror.

The telescope is able to rotate in azimuth only and during observations an object can be tracked by moving the SAC. As a result of the SAC motion the illumination of the SALT pupil will vary. The degree of vignetting also varies as a function field position (see Figure 2) as does the telecentric angle (see Figure 3).

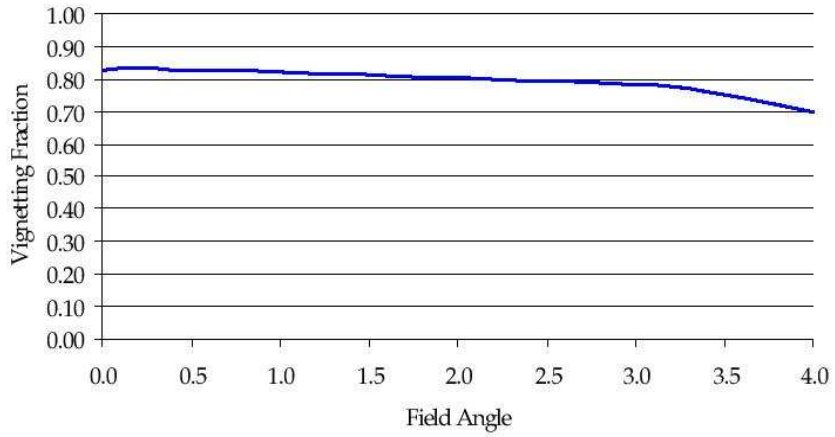

Figure 2: The vignetting at the SALT focal plane as a function of field angle (courtesy of N. Sessions).

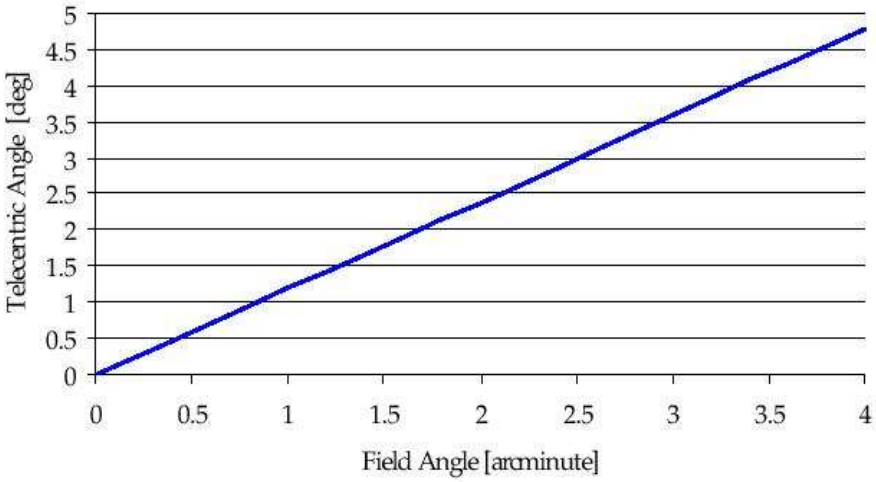

Figure 3: The telecentric angle at the SALT focal plane as a function of field angle (courtesy of N. Sessions). The range of the FIF will be limited to ±1 arcminute.

2.1 Fibre Instrument Feed

Details of the Instrument Feed (FIF) are given in SALT document 3400AE0024 FIF. The FIF will accommodate up to 12 individual fibres that are mounted in two rows of 6 fibres each. The two rows can be moved apart along a set of rails. A second pair of rails provides motion in the orthogonal direction. Five pairs of fibres are available for use by SALT HRS. Each pair of fibres can be separated anywhere from approximately 15 arcseconds to 1 arcminute. This will limit the variation in vignetting (Figure 2) and telecentric angle (Figure 3) between the two fibres.

2.2 SAC calibration optics.

A calibration system designed by Swat and Esterhuyse (Buckley et. al 2004) is able to mimic the illumination of the SALT focal plane. A schematic of one possible concept is shown in Figure 4. The calibration optics can be moved into the beam either immediately prior to or after and observation, or during the daytime. Light sources will exit a fibre bundle 8mm in diameter. SALT HRS requires at least a thorium argon lamp for wavelength calibration and a white lamp for flat-fielding and échelle order definition.

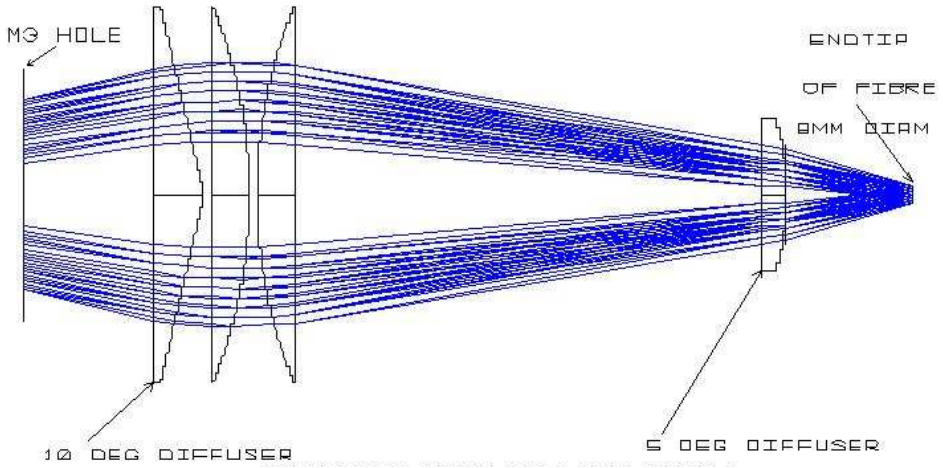

Figure 4: The SALT prime focus calibration system. The calibration light exits a 8mm diameter fibre bundle.

3 SALT HRS overview

The spectrograph is a dual beam white pupil design, with a single R4 échelle grating, a dichroic beam-splitter, and volume phase holographic grating cross-dispersers. The échelle grating has 41.6 grooves/mm and is illuminated with a 200 mm diameter beam. Two fully dioptric cameras are used to acquire complete wavelength coverage from 370 nm to 890 nm at a maximum resolving power of R = 70,000 and in a fixed spectral format. Two objects can be observed simultaneously with a minimum separation between adjacent orders of 11 arcsecs. The higher resolving powers are obtained by using dual fibre image slicers.

Apart from shutters, camera focusing, and the fibre interchange mechanism, SALT HRS will contain no moving parts. In order to provide complete immunity from pressure and temperature changes all optical elements (except the higher resolution fibre feed optics) will be enclosed with a light (~2 hPa) vacuum. The entire instrument will in turn be housed in a temperature stabilized environment.

A schematic of the optical layout of SALT HRS is shown in Figure 5. The three-dimensional layout of the spectrograph is more clearly seen in Figure 6 and the mechanical structure around these optics is shown in Figure7. Detailed properties of the blue and red arms of SALT HRS are given in Table 2 and Table 3. All parameters have been derived using the theory described in appendix 3210AE0034 optical appendix B.

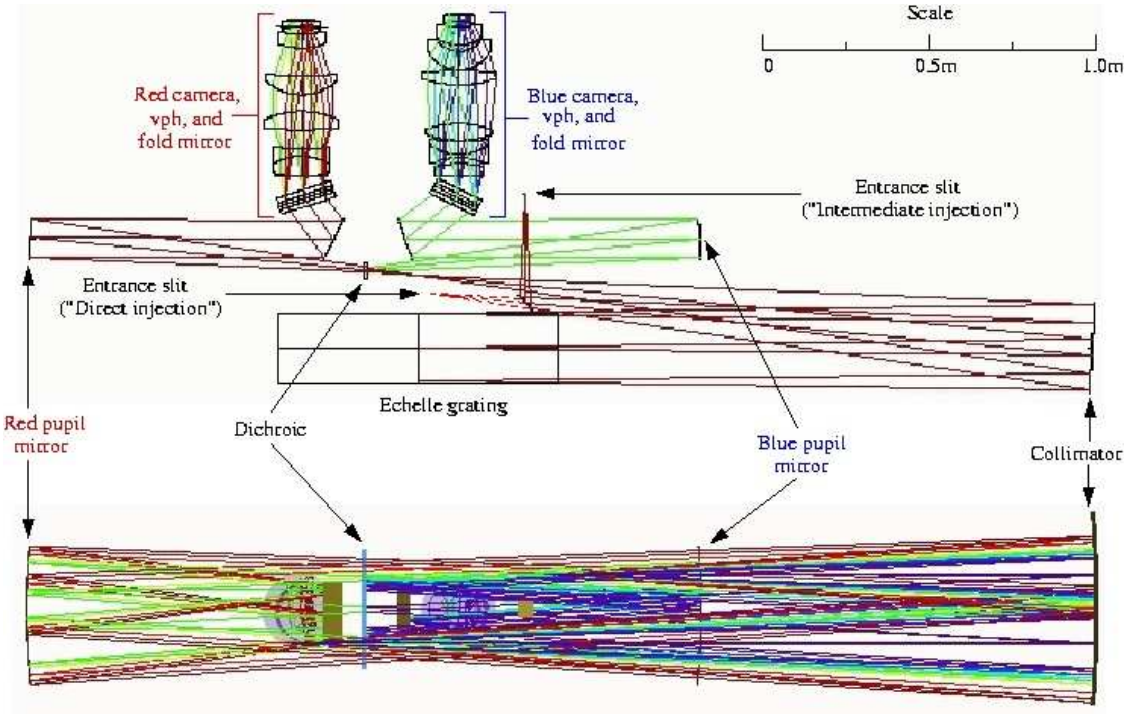

Figure 5: SALT HRS schematic overview of the optical design. The three-dimensional layout of the spectrograph is more clearly seen in Figure 6.

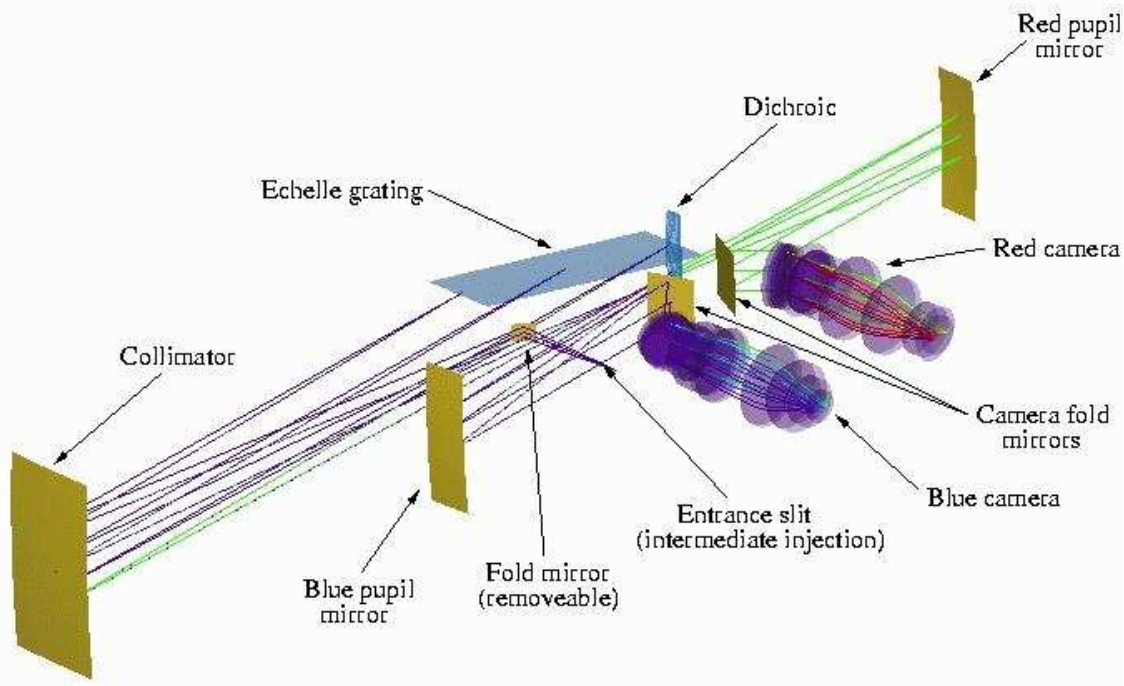

Figure 6: SALT HRS solid model of the optical elements.

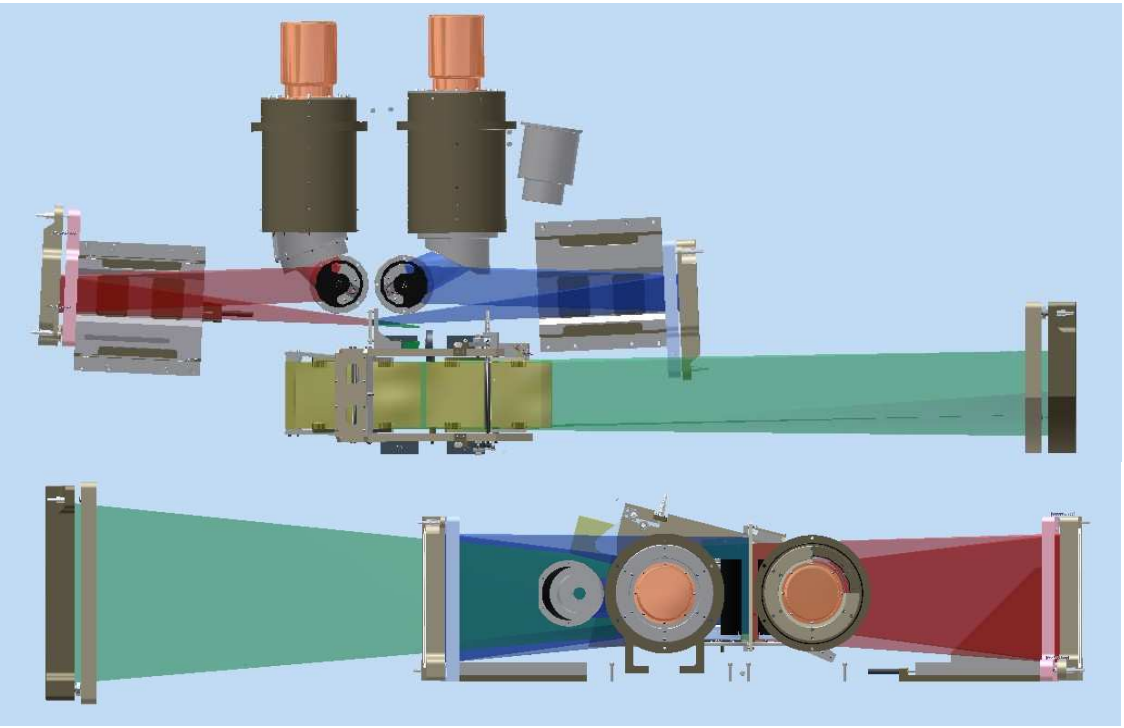

Figure 7: [Modify/label?] Plan (top) and elevation (bottom) of SALT HRS showing the optical elements and their mechanical mounts.

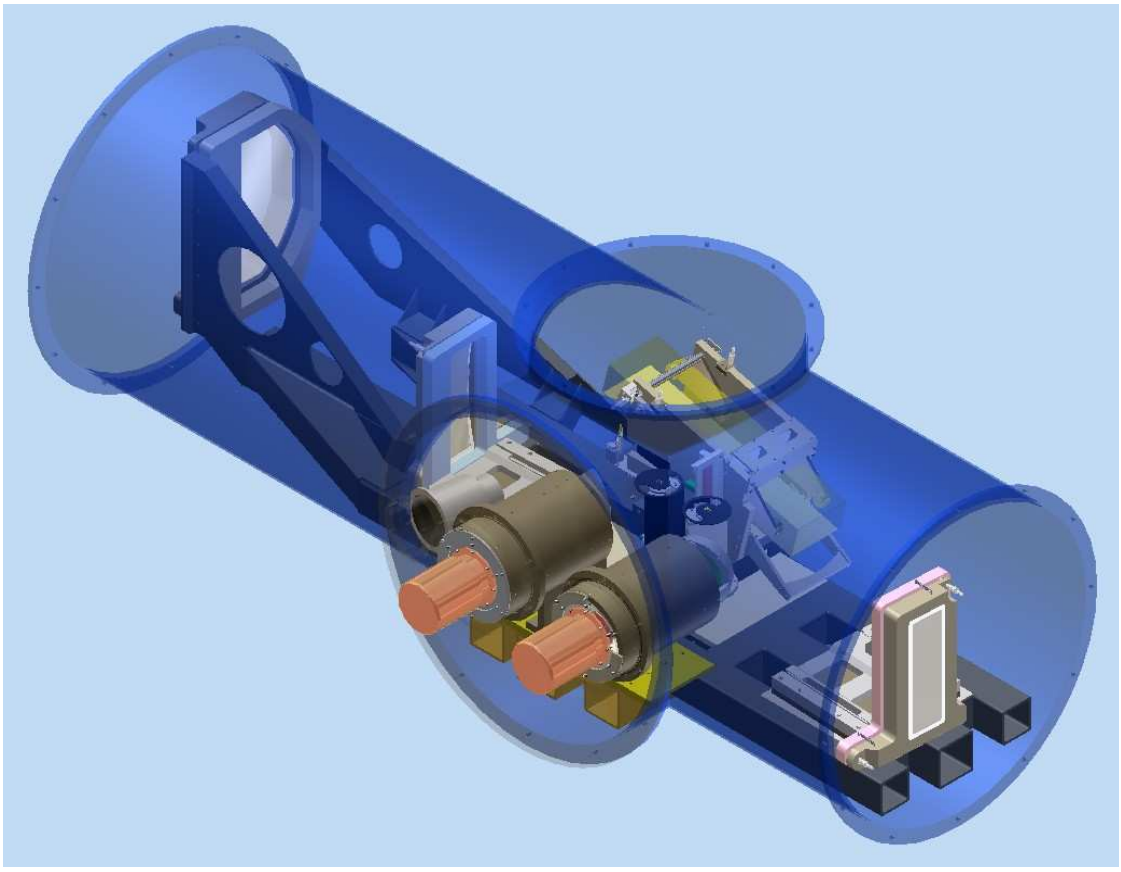

Figure 8: The mechanical structure and vacuum chamber around the optical elements. Collimator is at top left, red pupil mirror bottom right and the cameras are in the middle.

Table 2: Summary of SALT HRS blue arm properties.

```
Telescope: SALT
  D = 11.0m, f = 46.20m (f/D = 4.20)
  Plate scale = 224.0 um/arcsec (4.46 arcsec/mm)

Beam size: B = 200.0 mm
R_max        = 80000.0

Wavelength range: 373.3 to 555.5 nm
 (in 42 orders: m = 125 to  84)

Echelle grating:
  Blaze angle    = 76.00 deg (R4.01)
  Littrow angle  = 0.05 deg
  T              = 41.6 grooves/mm
  L x W          = 836.0 x 204.0 mm
  (no. gratings  = 2; each 410.0 x 204.0 mm, with 16.0mm gap)
  [T_blz,T_ove,T_gap] = [82.2,97.5,2.5]

Cross-dispersion/order separation:
  Method = Holographic grating
  Glass  = bk7
  T      = 1850 lines/mm
  thetai = 24.60 deg (lamB = 450.0 nm)
  coat   = mgf2 @ 30deg
  min = 10.5 arcsec, max = 26.5 arcsec

Collimator:
  F  =  3.82, f  =  763.6 mm
  (assumes B = 200.0, f/D_tel = 4.2 and FRD rho = 1.10)
  F1 = 10.00, f1 = 2000.0 mm
  Plate scale = 586.6 um/arcsec (1.70 arcsec/mm)

Camera:
  F  =  1.50, f  =  166.8 mm
  (assumes 2.0 (15.0um) pixel sampling of R_max
   and pupil demagnification cam_dmag = 1.8)
  Plate scale =  88.1 um/arcsec (11.36 arcsec/mm)

CCD:
  Type        = ccd44_82
  Coat        = E2V StdSi astroBB
  n_pix [x,y] = [2048,4096] pixels
  s_pix       = 15 microns
  num   [x,y] = [1,1] (y)
  Pixel scale = 5.9 pix/arcsec (0.17 arcsec/pix)
```

Table 3: Summary of SALT HRS red arm properties.

```
Telescope: SALT
  D = 11.0m, f = 46.20m (f/D = 4.20)
  Plate scale = 224.0 um/arcsec (4.46 arcsec/mm)

Beam size: B = 200.0 mm
R_max        = 100000.0

Wavelength range: 548.9 to 880.4 nm
 (in 33 orders: m =  85 to  53)

Echelle grating:
  Blaze angle    = 76.00 deg (R4.01)
  Littrow angle  = 0.05 deg
  T              = 41.6 grooves/mm
  L x W          = 836.0 x 204.0 mm
  (no. gratings  = 2; each 410.0 x 204.0 mm, with 16.0mm gap)
  [T_blz,T_ove,T_gap] = [75.2,97.5,2.5]

Cross-dispersion/order separation:
  Method = Holographic grating
  Glass  = bk7
  T      =  855 lines/mm
  thetai = 17.54 deg (lamB = 705.0 nm)
  coat   = mgf2 @ 30deg
  min = 10.8 arcsec, max = 24.7 arcsec

Collimator:
  F  =  3.82, f  =  763.6 mm
  (assumes B = 200.0, f/D_tel = 4.2 and FRD rho = 1.10)
  F1 = 10.00, f1 = 2000.0 mm
  Plate scale = 586.6 um/arcsec (1.70 arcsec/mm)

Camera:
  F  =  1.88, f  =  208.5 mm
  (assumes 2.0 (15.0um) pixel sampling of R_max
   and pupil demagnification cam_dmag = 1.8)
  Plate scale = 110.1 um/arcsec (9.08 arcsec/mm)

CCD:
  Type        = fairchild ccd486
  Coat        = Fairchild broadband
  n_pix [x,y] = [4096,4096] pixels
  s_pix       = 15 microns
  num   [x,y] = [1,1] (y)
  Pixel scale = 7.3 pix/arcsec (0.14 arcsec/pix)
```

4 SALT HRS detailed design

The following subsections contain detailed descriptions of the optical elements following the light path through the instrument.

4.1 Fibre injection

4.1.1 Telescope input

The input into the SALT HRS fibre injection for all proposed observing modes occurs at the Fibre Instrument Feed (FIF) which is located at the SALT prime focus (see 3400AE0024 FIF).

Several pair of fibres is required to service the fibre injection modes listed below. Each fibre pair will be mounted in input ferrules as specified in the FIF CDR document 3400AE0024 (their Figure 10, repeated as Figure 9 in this document). To limit reflection losses the input face of each fibre will be cemented to a fused silica entrance window that will be multi-layer over-coated. This window will be 0.5mm thick and 3-4 mm in diameter. Note that the input fibre ferrule must be adapted to accommodate this window [**TBC**]. The original ferrules are shown in Figure 10.

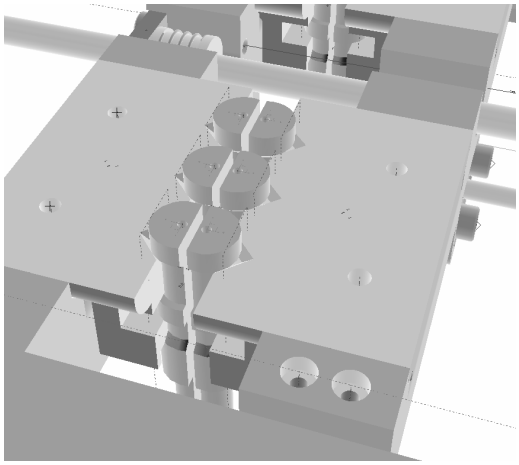

Figure 9: Mechanical model of the FIF cradles showing three of the six pairs of fibre input ferrules (from 3400AE0024 FIF).

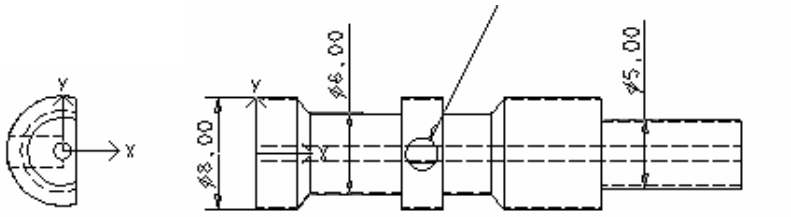

Figure 10: Mechanical drawing of the input fibre ferrule. Note that the input end of the fibre ferrule must be adapted to accommodate the entrance window.

4.1.2 Spectrograph input

Two possible paths for injecting light into SALT HRS will be possible. These are:

1. **Direct injection**. In this mode, fibres will be placed inside the spectrograph at the focus of the collimator.

2. **Intermediate injection**. These modes requires the use of transfer optics to firstly reimage the fibre exit faces onto an image slicer and secondly onto a slit plate inside the spectrograph.

The location of each input is shown schematically in Figure 9. The two available entrance positions are at the focus of the off-axis collimator and selected by means of an approximately 45 degree fold mirror that can be positioned in or out of the direct beam. Each of the modes will be described in more detail below.

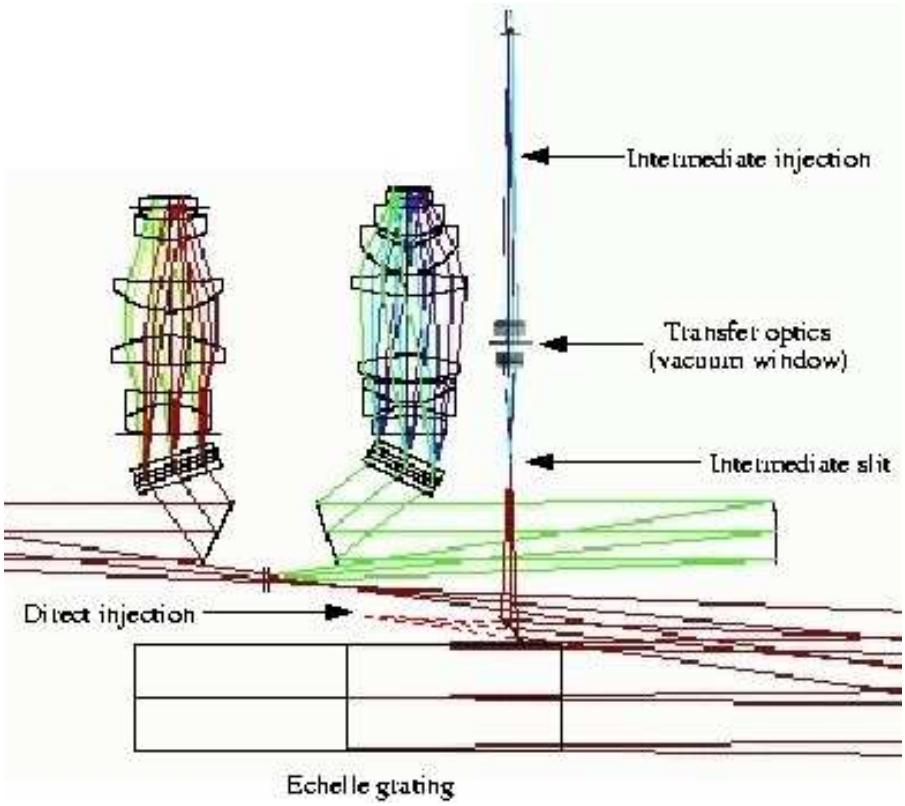

Figure 11: Schematic of SALT HRS showing the location of the direct and intermediate fibre injection.

Direct injection

For this input, fibres will be positioned at the direct collimator focus. Initially five fibres will be placed here. These are:

- 2 x 500 μm fibres – low resolving power object plus sky.
- 2 x 500 μm fibres – spare object and/or sky.
- 1 x 100 μm fibre – reference calibration fibre.

Each fibre (including the calibration fibre) will be coupled to a micro-lens to convert the nominal f/3.8 focal ratio emerging from the fibre to f/10. The micro-lens will reimage the near-field of the 500 μm fibres onto the échelle grating. The 100 μm calibration fibre will not use pupil-imaging and will be available for use with a laboratory emission line source only. This lens grouping can be seen schematically in Figure 12 and Figure 13.

Each micro-lens (except for the 100um fibres' lens) will be housed inside a thin-walled ferrule to prevent cross-talk. The convex surface of each micro-lens is to be anti-reflection coated with a multi-layer coating. The separation between the 500 μm fibres is 3.6″ (2.1 mm) on each side or 5.1″ on a diagonal.

The low resolution fibre are able to be used in a nod and shuffle mode for high accuracy subtraction of the sky background.

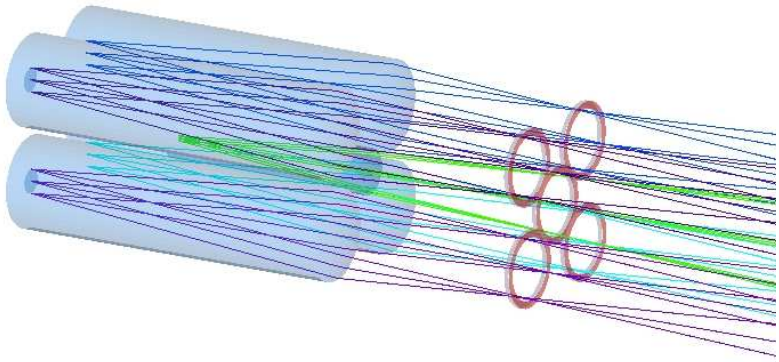

Figure 12: Schematic of the direct fibre injection. Four 500 μm fibres are coupled to each micro-lens and a fifth 100 μm fibre is coupled to another micro-lens in the middle. The rings to the right of this image represent the location of an aperture stop.

Figure 13: Schematic plan (left) and elevation (right) of the direct injection micro-lenses. The plan shows the grouping of the four 500 μm fibres and their micro-lenses with a fifth 100 μm fibre and smaller micro-lens in the middle.

Intermediate injection

This position will provide for interchangeable fibre injection options. A focal plane has been provided which is reimaged by a set of transfer optics onto an intermediate slit. Initially, only fibre image slicers will be used by SALT HRS in the intermediate injection position. These will provide for a medium and a high resolution observing mode. A schematic of the fibre interchange mechanism is shown in Figure 14. Space for six interchangeable inputs will be provided on the selector. Only three of these positions are presently assigned.

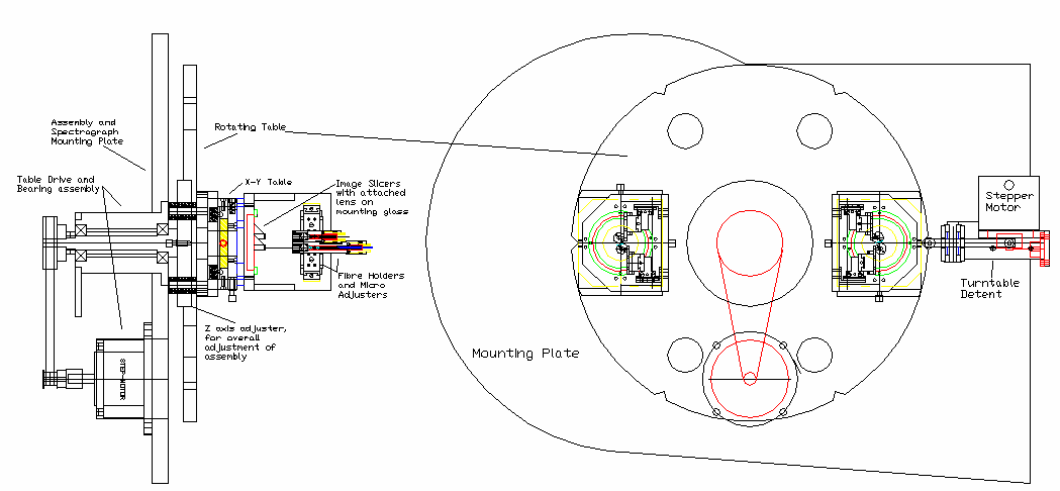

Figure 14: The fibre interchange mechanism for SALT HRS. For details see 3230AE0030 Input Mechanical Design.

An overview of the intermediate injection optics is shown in Figure 15. The transfer optics have been designed to accommodate the f/25 output from the image slicers and to reimage at f/10 (the collimator focal ratio) onto the slit plate. The transfer optics comprises two N-FK51/S-LAL7 doublets (Figure 16). Between these doublets is a plane-parallel silica window into the vacuum tank. A telecentric corrector is located just behind the slit plate (Figure 17).

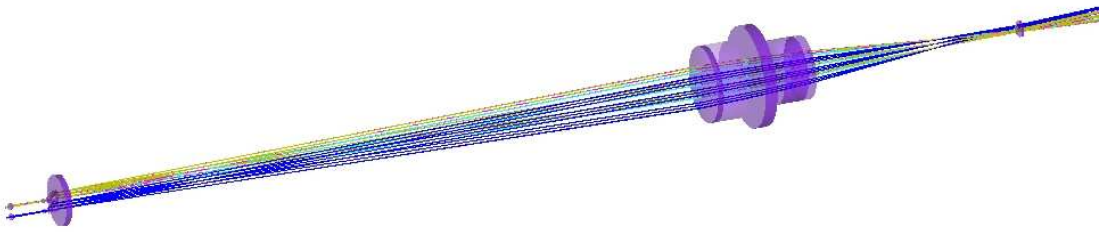

Figure 15: The intermediate injection optics. A fibre image slicer provides the input (left) and focal conversion optics (centre) transfer the sliced image onto the slit plate (right). A telecentric corrector immediately behind the slit plate corrects the input into the spectrograph.

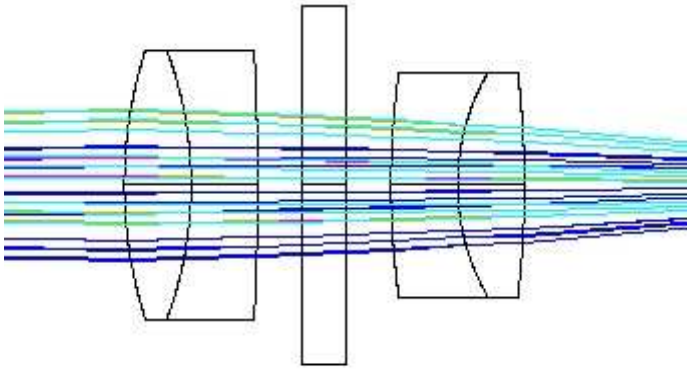

Figure 16: The intermediate slit transfer optics.

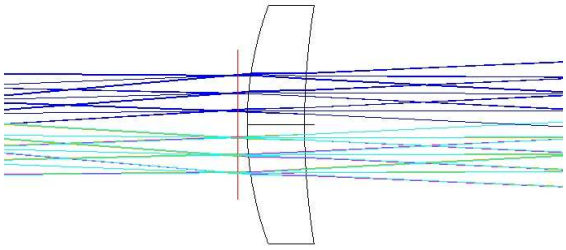

Figure 17: The intermediate slit telecentric corrector.

Two fibre-sliced modes will be available. Each mode will require two pairs of fibres. These are:

- 2 x 500 μm fibres – medium resolving power object plus sky.
- 2 x 350 μm fibres – high resolving power object plus sky.

The fibres will have 0.5mm thick silica plates bonded to both the input and output faces. These plates are able to be multi-layer overcoated.

The f/3.8 output beam from each fibre is converted to f/35.5 using a COTS BK7 ball lens 5mm in diameter. A custom LAL7/silica doublet bonded to each image slicer entrance face reduces this to f/25. Splitting the focal conversion in this manner allows for a (required) telecentric image of the fibre exit on the image slicer. Each dual-beam image slicer comprises two prisms plus two thin slicer plates all of which are silica. The optical scheme is shown in Figure 18 and Figure 19.

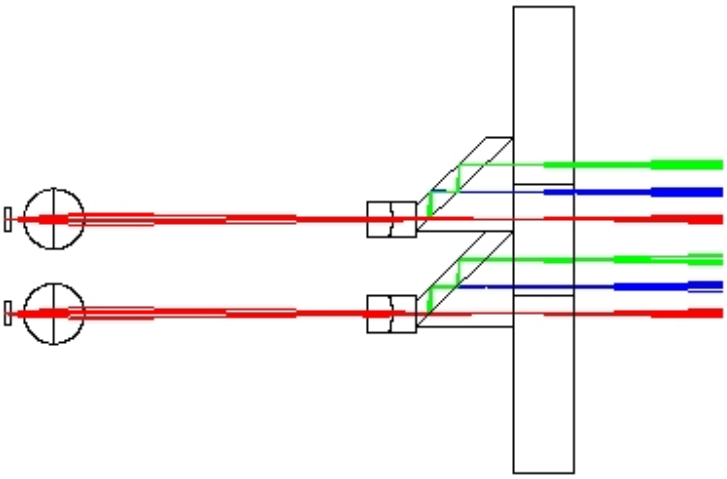

Figure 18: Fibre image slicer for SALT HRS. Shown is the high resolving power slicer. The medium resolving power image slicer is similar.

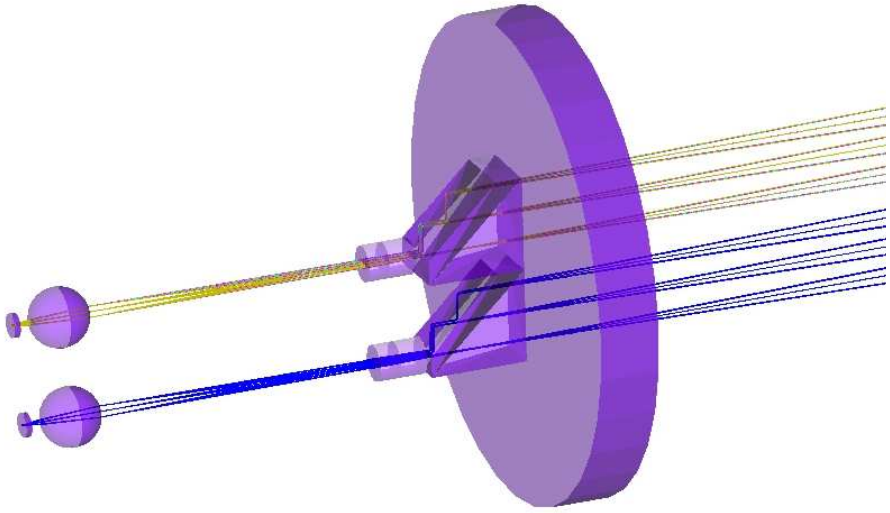

Figure 19: Solid model of the high resolving power fibre image slicer.

After exiting the image slicer, each circular image of the fibre exit has been cut into three slices, stacked end to end. Images of the medium and high resolving power sliced fibres are shown in Figure 20. These images are shown after being reimaged by the transfer optics. Each image will be precisely located onto a slit plate (Figure 21). As well as providing for a very stable entrance slit for SALT HRS, the slit will prevent stray light from the image slicer from entering the spectrograph. Light reflected off the front surface of the image slicer will be used by the slit viewing optics (see below) to align the fibres onto each slicer, and the sliced images onto the slit.

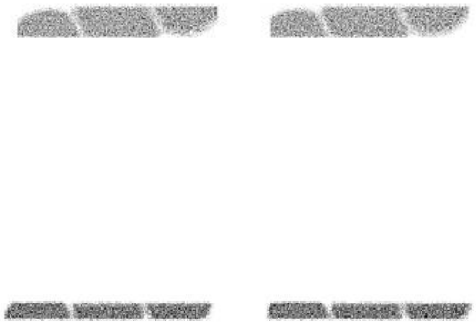

Figure 20: Images of the medium (left) and high (right) resolving power sliced fibres. The image plane is immediately behind the slit plate shown in Figure 21.

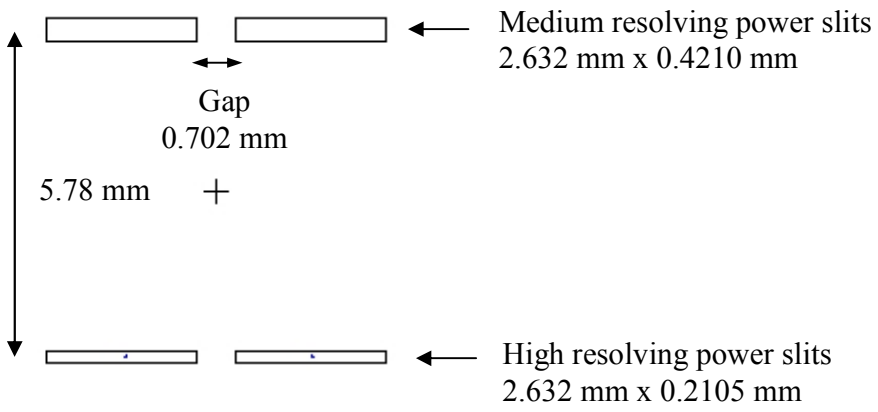

Figure 21: Slit plate layout.

Summary of input modes

A summary of the SALT HRS fibre feed input modes is given in Table 4.

Table 4: Summary of the SALT HRS fibre feed formats. In each mode a single object plus sky can be observed.

Spectrograph fibre feed mode	***Description***	D_{fibres} ***(µm)***	N_{slices}	W_{slices} ***(µm)***	H_{slices} ***(µm)***	***Resolving power****
High IS	High resolving power image slicer	350	3	80	333	65000
Med IS	Medium resolving power image slicer	500	3	160	333	37000
Low	Low resolving power fibre	500	-			16000
Ref. fibre	High resolving power fibre (reference fibre only).	100	-			~70000

*resolving powers are for a single wavelength in the centre of each CCD.

4.2 Collimator

The collimator mirror (M_1) is used first as a collimator and then after échelle dispersion as a pupil transfer mirror. The mirror is an *f*/10 off-axis paraboloid. This choice of focal length is a compromise between an excessively large instrument (i.e., slow focal ratio), and a tolerably fast focal ratio which can be readily manufactured. In order to accommodate the dual use of the collimator as the first pupil transfer mirror, the total aperture must be 270 mm × 570 mm. The mirror can be sourced from a 690 mm diameter parabolic parent with a 4000 mm radius of curvature (see Figure 22).

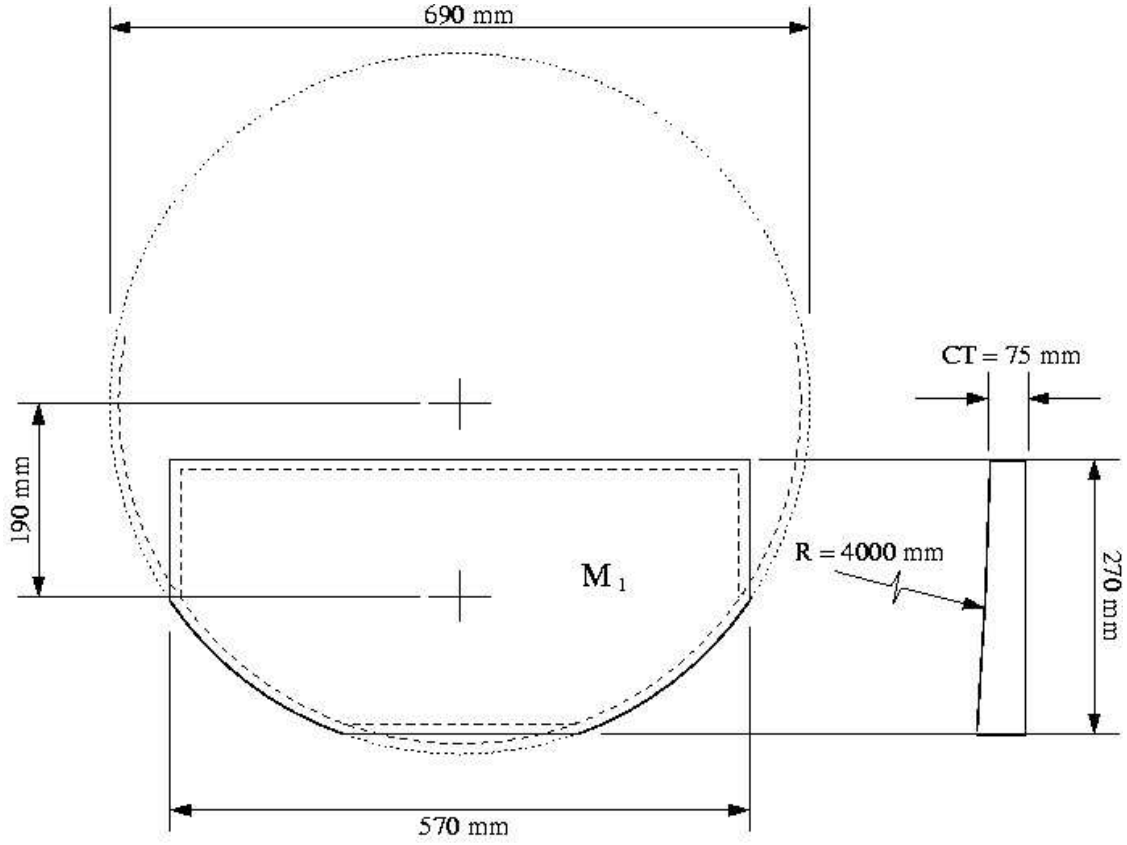

Figure 22: Collimator (M_1) dimensions. The clear aperture is indicated by the dashed line.

4.3 Echelle grating

SALT HRS will use a single échelle grating with 41.59 g/mm and a 76° blaze angle for primary dispersion. The grating will be formed from a mosaic of two approx. 204 x 407mm segments replicated onto the surface of a single 214mm x 840mm x 125mm Zerodur substrate. The gap between segments will be at least 15mm.

The collimator (see above) is designed to deliver a 200mm collimated beam onto the grating, which assuming fibre FRD of 10%, ensures there will be no overfilling. About 5% of incident light will be reflected off an aluminized mylar strip placed between the two grating segments and collected by exposure meter optics. Overfilling of the grating will occur at non-zero telecentric angles into the fibre input. This effect is summarized in Table 5. A similar loss is to be expected if fibres with significantly worse FRD (e.g. 20%) are used instead.

Table 5: A summary of the effect of telecentric angle on echelle overfilling and telescope vignetting. Fibre, collimator, etc losses are not considered here.

Field angle	Telecentric angle	Effective focal ratio		Effective beam size	Transmission due to:		
		Input	Output	(mm)	Overfilling	Vignetting	Total
0′	0°	f/4.2	f/3.8	200	95%	84%	80%
1′	1.2°	f/3.6	f/3.3	230	87%	82%	71%

The grating will be illuminated in quasi-Littrow mode; i.e $\theta \approx 0°$ and $\gamma \neq 0$. The angle of illumination with respect to the grating facet normal will be approx. $\theta \approx 0.3\text{-}0.5°$. The exact value will be determined during commissioning in order to precisely centre the blaze function on the CCD. This will also accommodate the tolerance in the grating blaze angle.

Following echelle dispersion, each dispersed beam returns to the off-axis collimator. The mirror now acts as the first transfer mirror of the white pupil system and forms an intermediate image at the mirror's focus. This image is at a location just offset from the direct injection input. The splitting of the spectrograph into red and blue arms by a dichroic filter occurs just after the intermediate focus.

4.4 Dichroic

The blue and red arms of SALT HRS are separated by a dichroic which has a wavelength division of 550nm. The dichroic splitting takes place 150mm after the intermediate focus of the white pupil transfer system. Splitting allows SALT HRS to make use of a single echelle grating but consequently this makes the size of the dichroic quite large (see Figure 23) as it must cope with an ~f/10 image of the echelle spectrum. The efficiency of the dichroic can be maximised by limiting the angles of incidence to values near zero and by using the blue wavelengths in reflection and the red wavelengths in transmission.

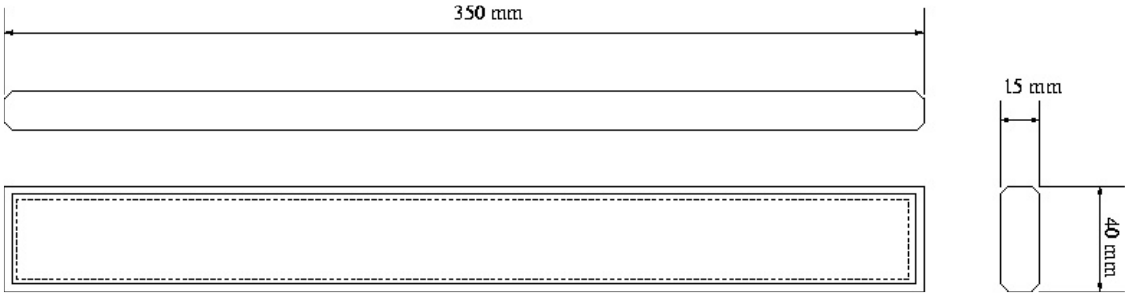

Figure 23: The dimensions of the dichroic. The clear aperture (dashed line) is 340 mm x 30 mm.

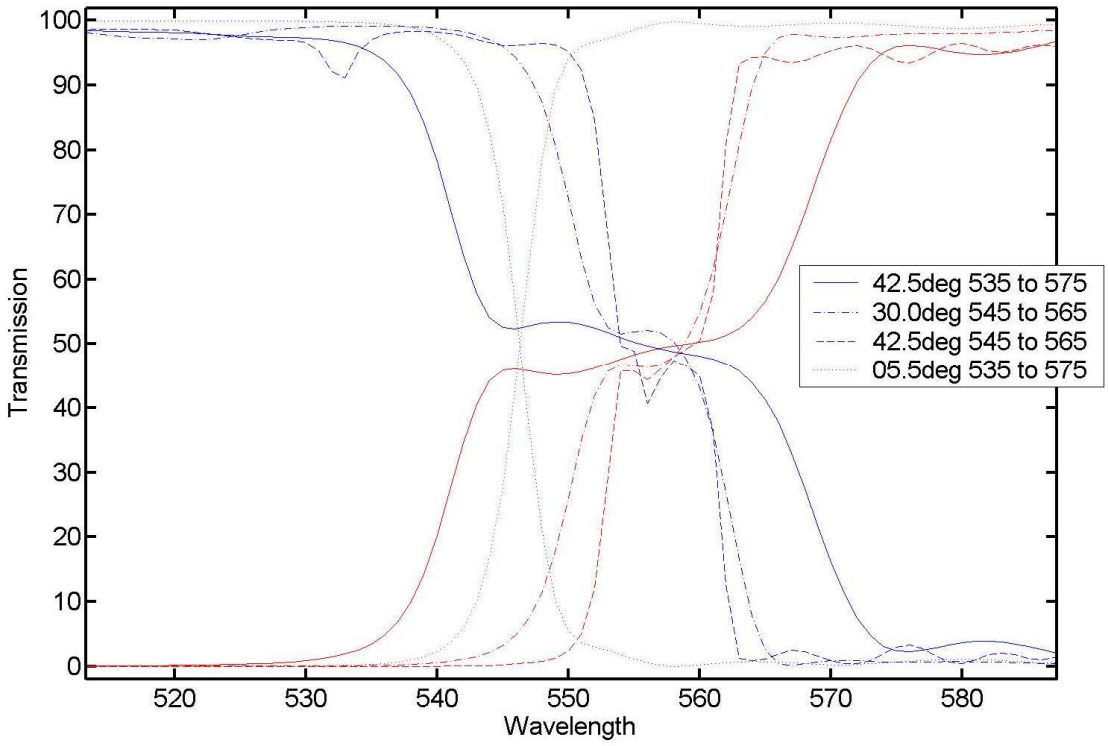

Figure 24: The efficiency of the SALT HRS dichroic near the cross-over wavelength. The dichroic will be used at an angle of incidence of 5.5 degrees to minimize the cross-talk between spectrograph arms. Calculations are by Barr Associates.

4.5 Blue and red pupil mirrors

The blue and red pupil mirrors are used in conjunction with the collimator mirror to reimage the pupil from the echelle grating onto the VPH gratings. The focal length of these mirrors is chosen so that the reimaged pupil is 1.8 times smaller than the pupil on the echelle. That is, by using a mirror with a 1111.1mm focal length the final pupil size will be 200/1.8 = 111.1mm (neglecting echelle anamorphism).

By demagnifying the pupil it is possible to significantly decrease the size of the camera optics. However, there are practical limits to the amount of demagnification. The field of view of the camera is inversely proportional to the demagnification. An extremely small camera would require an excessively large field of view and correspondingly more difficult optics (even if they are smaller). The chosen demagnification factor of 1.8 is a compromise between the factor of 2 suggested by Bernard Delabre at the 2004 September PDR and earlier SALT HRS camera designs which had unity magnification. It was found that this removed the apparent need for a doublet field-flattening lens and eased the constraints on the form the two other large doublets.

Both the blue and red mirrors are identical spherical mirrors (except for their coatings) (see Figure 25). Each mirror is placed 20 to 30mm further from the intermediate focus than its focal length. This means that the pupil is not formed in exactly collimated light. To correct for this the VPH gratings will be immersed in a pair of lenses and these and the pupil mirrors have been designed as an integrated part of the imaging system.

The pupil mirrors will serve as the active focusing element of SALT HRS. The temperature and pressure stability of SALT HRS will limit the need to refocus and as shown in Section 5.3 a ±1mm shift in pupil mirror focus can compensate for the thermal expansion resulting from a change in temperature from 15 to 25 °C. The pupil mirror focus is also needed to compensate for the change in focus from atmospheric pressure to a vacuum. This is possible with a 6.2mm shift in the blue mirror and a 5.7mm shift in the red.

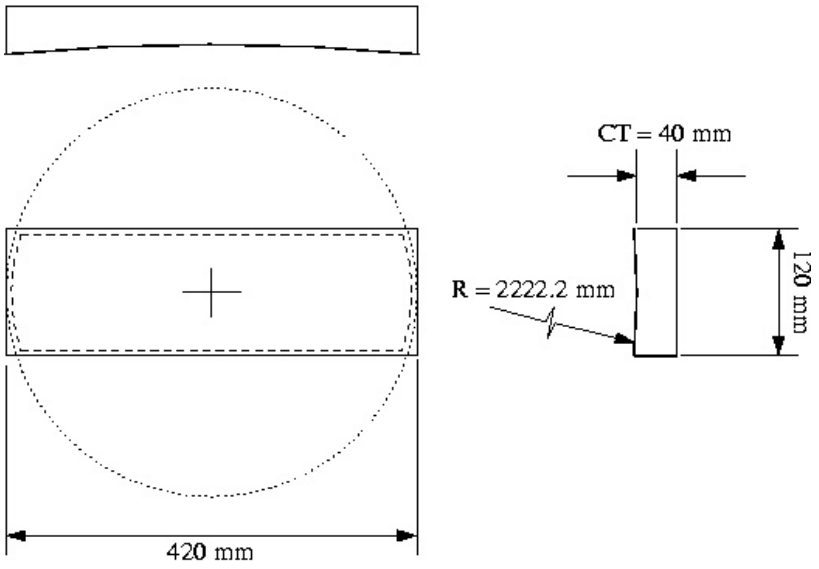

Figure 25: Blue and red pupil mirror dimensions.

4.6 Fold mirrors

The use of a dichroic to split SALT HRS into two beams allows a large number of potential spectrograph formats to be explored. However, as noted above, the efficiency of the dichroic is maximised by limiting the angles of incidence to values near zero. Therefore, in order to avoid a conflict between the blue and red cameras one (or both) spectrograph arms must use at least one additional fold mirror. Various fold options were explored which all had potential merits. The decision to adopt the layout presented here was made in conjunction with mechanical considerations. In particular, it is noted that having both camera focal planes in close proximity to each other and to the intermediate injection optics is desirable for enhanced mechanical stability since all three components may be mounted on a single structure.

4.7 VPH gratings

SALT HRS will use volume phase holographic (VPH) gratings in both the blue and red arms for cross-dispersion. The development of VPH gratings and their potential for use in astronomical instrumentation has been described by Barden et al (2000). A report by Clemens and Seagroves (1999) gives an overview of the theory of VPH gratings and an extensive list of technical information can be found on the NOAO VPH website[1].

The parameters of the VPH gratings have been optimized in order to provide the maxium possible order separation while maintaining complete wavelength coverage. The gratings will be located at the white pupil formed by the blue and red pupil mirrors. As was described above, these mirrors demagnify the entrance pupil by a factor of 1.8, and therefore each grating must be ruled a factor of 1.8 denser than if the magnification were unity. This works in favour of VPH gratings since those with low line densities become difficult to manufacture and are potentially less efficient.

A summary of the VPH grating parameters is given in Table 6. The grating substrate and cover glasses are both to be made from 10mm thick pieces of BK7. Each grating will have matched pairs of plano-concave and plano-convex lenses cemented to their surface. These lenses correct for the slight decollimation at the white pupil.

Table 6: Parameters of the VPH gratings for SALT HRS.

Grating	Line density *T* (lines/mm)	Wavelength range (nm)	Clear diameter (mm)	Substrate diameter (mm)
Blue:	1850	$370 < \lambda < 555$	134	150
Red:	855	$555 < \lambda < 890$	134	150

[1] http://www.noao.edu/ets/vpgratings/

4.8 The cameras

The blue and red arm cameras for SALT HRS are shown in Figure 26 and Figure 27. The designs are based on camera designs suggested by Bernard Delabre as starting points for SALT HRS. Both cameras show residual spherical aberration when imaging a perfectly collimated source. This is to be expected because they are optimised (along with the VPH lenses) to balance severe astigmatism and spherical aberration from their second, spherical, pupil mirrors

4.8.1 Blue camera

The blue camera has a focal length of 166.8mm. Assuming a detector with 15μm pixels, this allows for Nyquist sampling of a maximum resolving power of R = 80,000. The plate scale is 88μm/arcsec (or 11.36 arcsec/mm). The detector area is 30.7mm x 61.4mm which implies a camera field of view of ±11.6° on a diagonal.

The first element of the blue camera (BCM1.1) has a conic surface. An alternative would have been a sixth order even asphere. Both surfaces would have had similar aspheric departures but a conic only surface is potentially easier to manufacture. This element is made from S-FPL51Y; a somewhat expensive glass shared by only one other element (BCM3.1). The doublet BCM2.1/2.2 will be formed from PBM2Y/S-FSL5 which have nearly matching coefficients of thermal expansion. All other elements except the field-flattening lens are made from PBM2Y. The field-flattening lens is a singlet made from silica. The lens will be circular and the surface facing the detector is cylindrical. This lens will also serve as the window into the CCD cryostat. The centre of the field-flattening lens is 6.4mm from the CCD. All camera elements are coaxial with no tip or tilt. The total path length of the camera is 480mm and the maximum lens diameter is 220mm. Clear apertures will capture 99.5% of all rays assuming a uniform entrance pupil for all wavelengths across a single free spectral range. The wavelength range is from 370nm to 550nm.

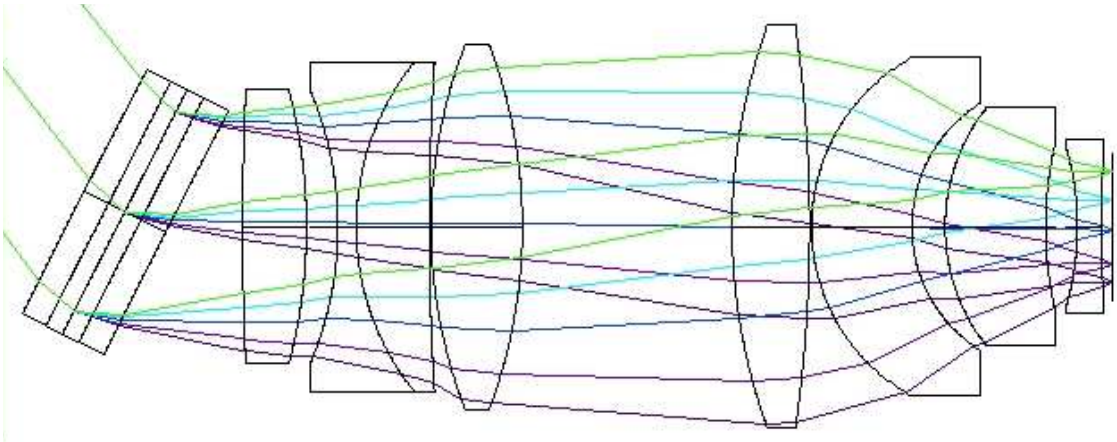

Figure 26: The blue camera for SALT HRS. The VPH grating (left) is also shown. The camera has a focal length of 166.8mm and the maximum diameter is 220mm.

4.8.2 Red camera

The red camera has a focal length of 208.5mm. This allows for Nyquist sampling of a maximum resolving power of R = 100,000, again assuming a detector with 15μm pixels. The plate scale is 110μm/arcsec (or 9.08 arcsec/mm) and the detector area is 61.4mm square. The field of view of the red camera is nearly identical to the blue; that is, 11.7° on a diagonal.

Again, the first element of the red camera (RCM1.1) has a conic surface. The form is very similar to that for the blue camera. The lens also forms part of a cemented S-FSL5/TIH1 doublet (RCM1.1/1.2), where each glass has a matching CTE. The two largest lenses (RCM2.1 & RCM4.1), are formed from S-BAH11 and BK7; both relatively inexpensive glasses. The largest element is 220mm in diameter. As in the blue camera, the field-flattening lens is made from a single piece of silica with one cylindrical surface located 8.3mm from the CCD. The red camera field-flattening lens will also be used as a CCD cryostat vacuum window. The total path length through the camera is 470mm.

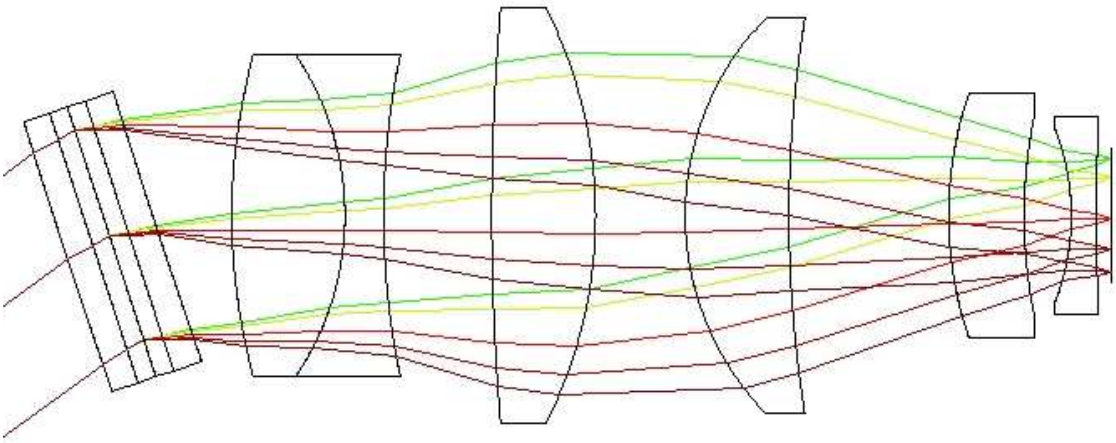

Figure 27: The red camera for SALT HRS. The VPH grating (left) is also shown. The camera has a focal length of 208.5mm and the maximum diameter is 220mm.

4.9 CCDs

The specifications of the CCDs are described in the documents 3200AE0015 FPRD and 3290AE0001 detector specification. A single 2k × 4k chip with 15 μm pixels will be used in the blue camera and the red camera will use a single 4k × 4k CCD, again with 15 μm pixels. This is sufficient to just capture a single free spectral range in every order. In order to accommodate a nod and shuffle mode, the cameras must have their columns aligned in the direction of cross-dispersion. The blue camera pixel scale is 5.9 pixels/arcsec (or 0.17 arcsec/pixel) and the red camera pixel scale is 7.3 pixels/arcsec (or 0.14 arcsec/pix).

4.10 Exposure meter

The exposure meter will use light that is reflected off the gap between the échelle mosaics. A 200 x 10mm aluminized mylar strip placed across this gap reflects approximately 4% of the light toward a collector. The collector, which is a 150mm focal length parabolic toroid made from aluminium, directs the light toward a 6.4mm fused silica light guide. The coupling efficiency is maximized by placing a cylindrical plano-convex lens on the light guide's entrance. The output of the light guide will illuminate the photocathode of a cooled photomultiplier tube (PMT) placed outside the spectrograph enclosure.

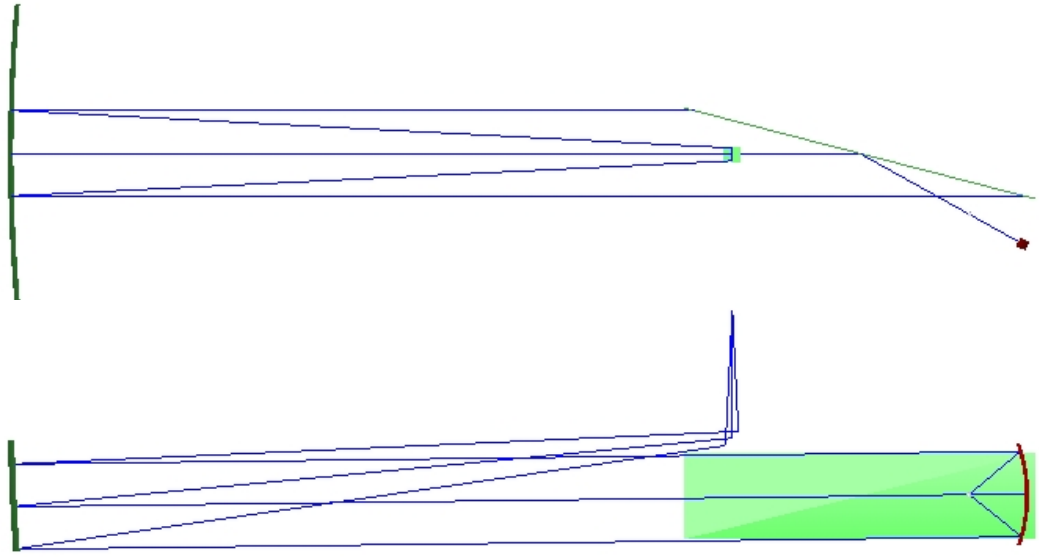

Figure 28: The exposure meter for SALT HRS uses light reflected off an aluminized mylar strip placed across the gap between the echelle mosaic. A fibre optic delivers the light to a PMT located outside the spectrograph enclosure.

It is noted that light off the exposure meter input light guide will be re-dispersed by the échelle and returned via the collimator mirror to the slit plate. The use of overcoated optics and a blackened rear surface of the slit plate will limit greatly reduce this light. Light that travels beyond the slit plate will not be able to redispersed.

4.11 CCD flat-fielding lamps

A schematic of the CCD flat-fielding system is shown in Figure 29. The flat-fielding source is a Dolan-Jenner DC-950 fibre optic illuminator which may be used with narrow-band filters. A 6.4mm dual branch light guide will couple the illuminator to the intermediate slit via a position on the fibre input assembly. The two light guides are then reimaged by the focal conversion optics onto the inputs of two fibre backlights located near the intermediate slit (see Figure 30). The entrance into the backlights will be via two small fold prisms to be positioned just in front of (but not obscuring) the slit plate (Figure 31). The fibre optic backlight is shown in Figure 32.

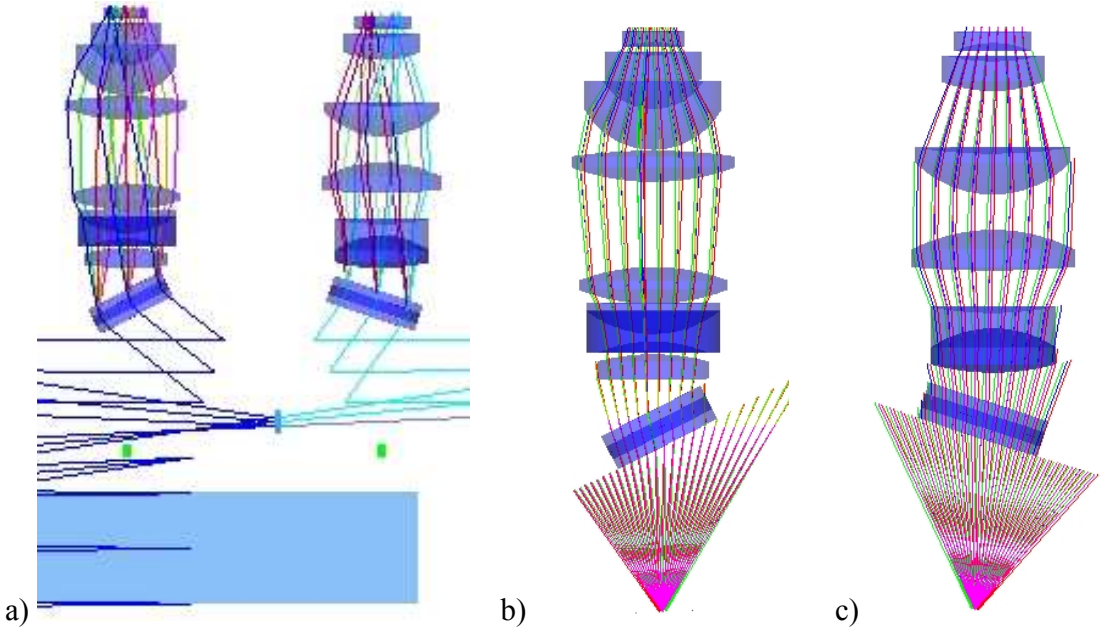

Figure 29: a) The location of the CCD flat-fielding lamps (green boxes). The illumination of the blue (b) and red (c) cameras is also shown.

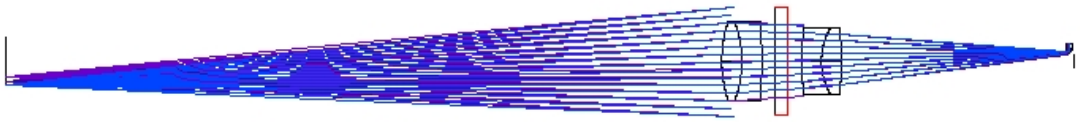

Figure 30: The input to the CCD flat-fielding illumination optics. A dual fibre bundle exits at (right, only one shown) and is reimaged by the intermediate slit transfer optics to a location near the slit plate. See Figure 31 for details.

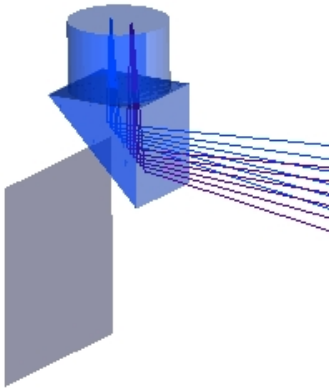

Figure 31: A small fold prism directs light into the fibre bundle (shown here by a small cylinder). The rectangle depicts the slit plate.

Figure 32: Fibre optic backlight from Edmund Scientific NT39-825.

4.12 Slit viewing optics

Sufficient space has been allocated to insert a 50/50 pellicle mirror into the light path between the image slicers and the intermediate transfer optics. Light that is reflected off the front polished face of the slit jaws will be returned back through the transfer optics and diverted by the pellicle mirror onto a CCD camera. The predicted image quality of this system (Figure 34) shows that it will be sufficient for aligning the fibre image slicers and for initial focusing. The optical scheme is shown in Figure 33. The CCD camera and doublet lens can remain fixed in place while the mirror must be able to move in and out of the beam.

The CCD will be a PULNiX TM-300 CCIR camera [**TBC**]. The detector uses a ½" interline transfer CCD with 752 x 582 pixels each 8.6µm x 8.3µm. Including interline masks, the detector has an area of 12.9mm x 9.7mm). The slit viewing optics operate at f/13 [**TBC**]

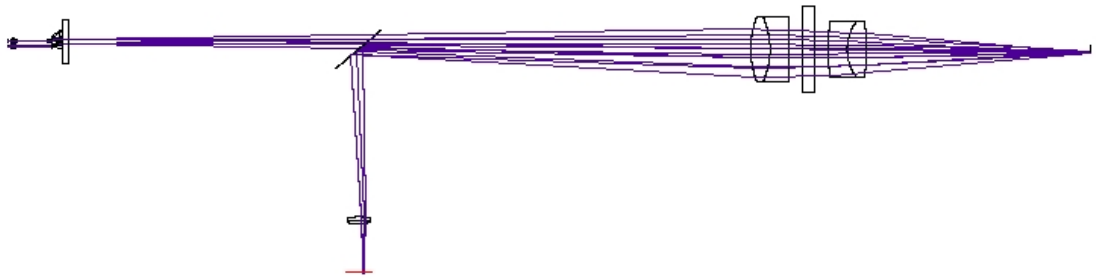

Figure 33: The slit viewing optics for SALT HRS.

Figure 34: An image of the highest resolving power sliced fibre using the slit viewing optics. Compare with Figure 20 above. The total length of the two slits is 8mm.

4.13 Baffles

Both the direct injection optics and intermediate injection optics require little additional baffling beyond that incorporated into their mountings. Baffles for the direct injection optics were described in Section 4.1.2 and will take the form of small aperture stopts located a short distance in front of each fibre's micro-lens. This will limit the fibre output focal ratio to f/3.8. The direct injection optics will have a baffle located on the vacuum window. The slit plate will eliminate any stay light from each of the fibre image slicers.

A schematic of some of the other baffles is shown in Figure 35. A narrow aperture will be placed at the location of the intermediate slit (see Figure 36) which will permit only those rays within one (far red) spectral range to pass.

Other baffles will be placed where appropriate. E.g., around the échelle grating, and between the two cameras.

The camera's themselves are effectively baffled masks which limit the clear apertures of each element (including the field-flattening lens and CCD).

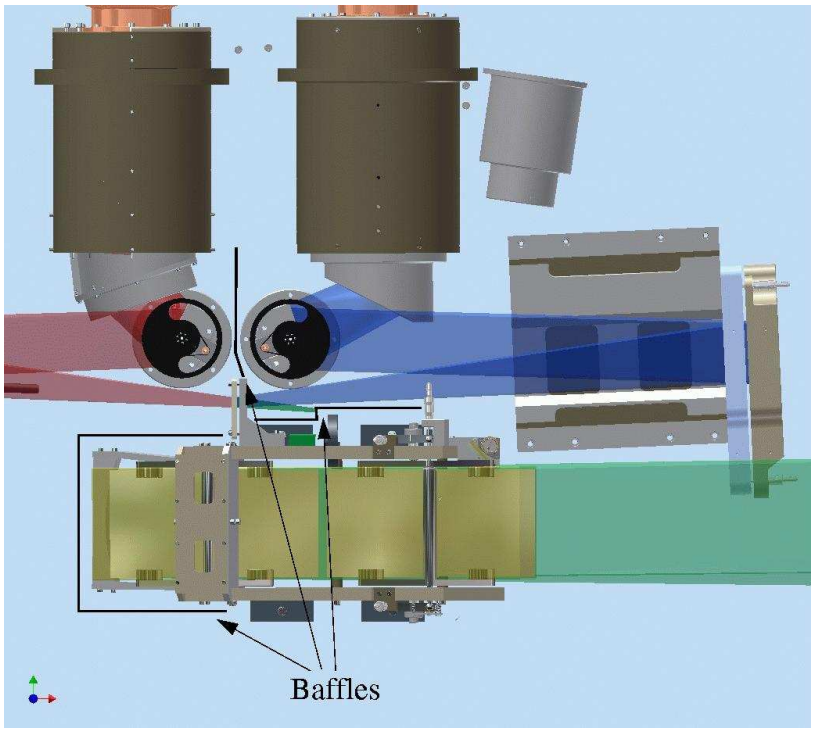

Figure 35: The location of some of the baffles for SALT HRS. The injection optics are not shown.

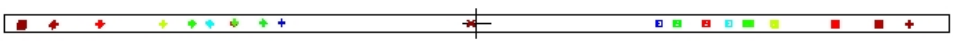

Figure 36: Intermediate slit aperture. The aperture is 310 x 6mm.

5 Performance

The analysis of the spectrograph's optical performance has been performed using the Zemax models listed in 3210AE0034 optical appendix A.

5.1 Spectral formats

The spectral formats in each of the two spectrograph arms are shown in Figure 37 and Figure 38. The choice of cross-dispersion line density, and dichroic cross-over wavelength has been optimised to ensure that complete wavelength coverage from 370 nm to 890 nm is obtained while maintaining the same minimum order separation in each arm. The spectral formats are based on detailed ray-tracing using the complete Zemax optical models. The exact CCD orientation (i.e., rotation) will be determined during the initial assembly phase.

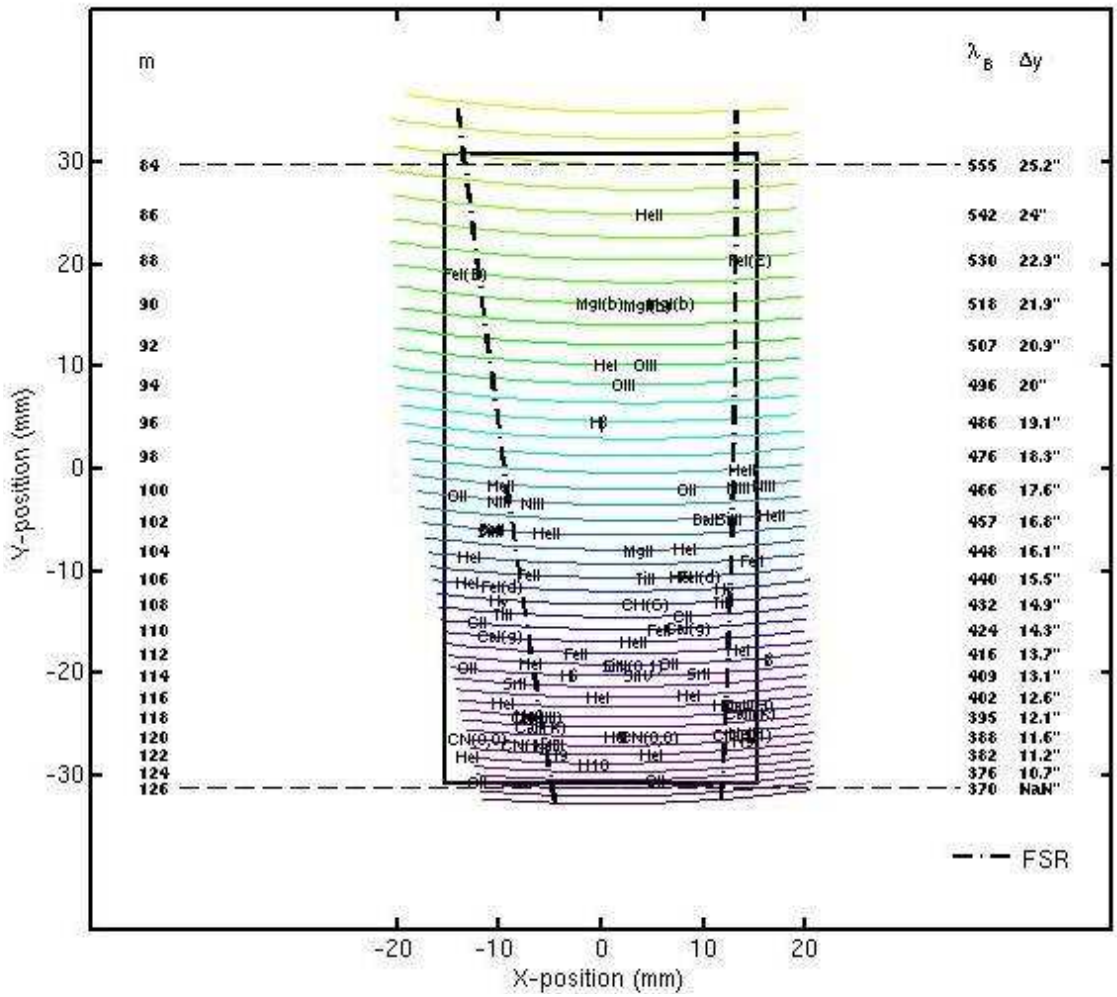

Figure 37: SALT HRS blue arm spectral format. The extent of one free spectral range is shown by the dashed lines. A single 2k by 4k detectors with 15 μm pixels is depicted by the bold rectangle. Labels correspond to the order centre.

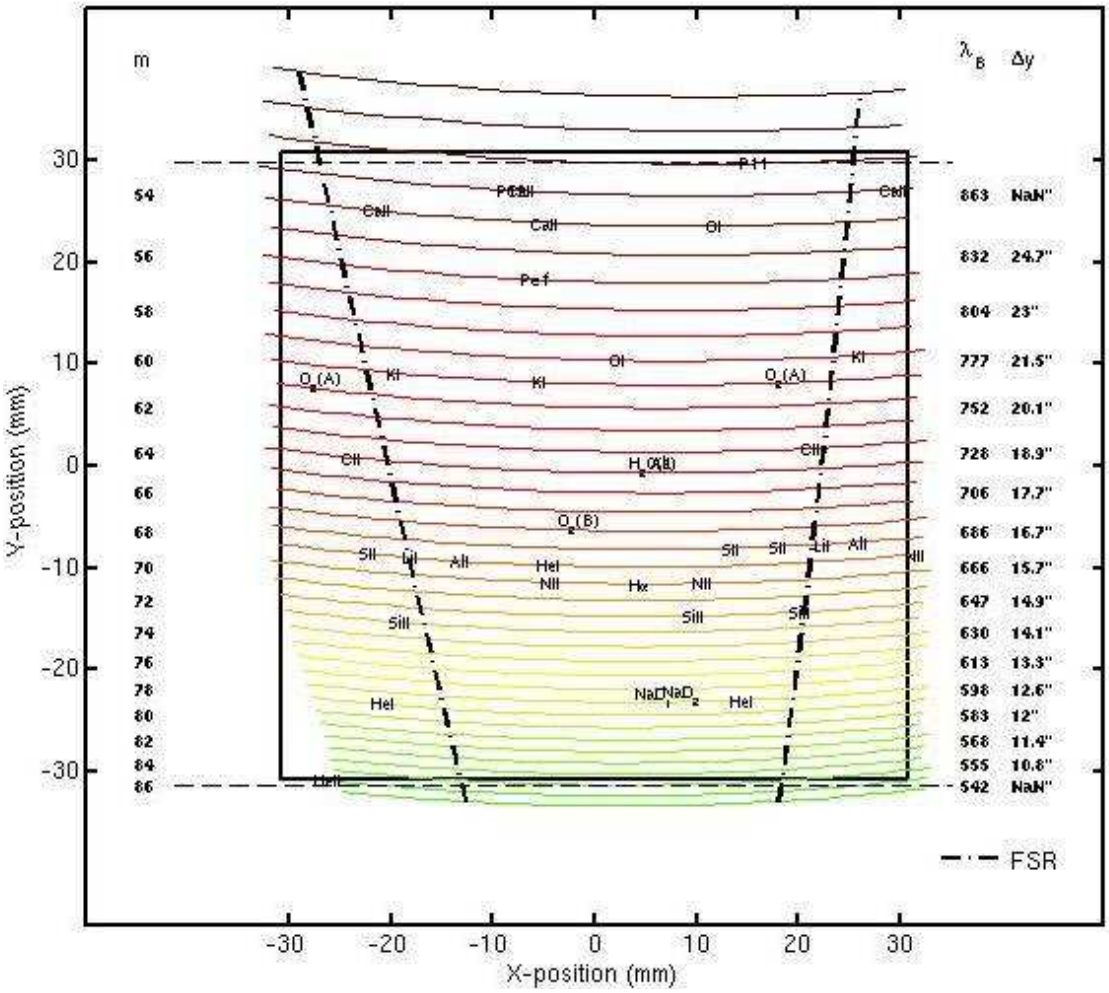

Figure 38: SAT HRS red arm spectral format. A single 4k by 4k detectors with 15 μm pixels is depicted by the bold rectangle. Labels correspond to the order centre.

5.2 Image quality

5.2.1 Slit optics

The image quality of the intermediate injection optics is shown in Figure 39. The optics are not quite diffraction limited at all wavelengths. However, 80% of the energy is enclosed within 80um, which corresponds to 0.14 arcsecs on the fibre input. This is two to three times the image quality of the spectrograph optics and is therefore adequate. Figure 40 shows an image of the medium and high resolving power sliced fibres as seen from the slit plate.

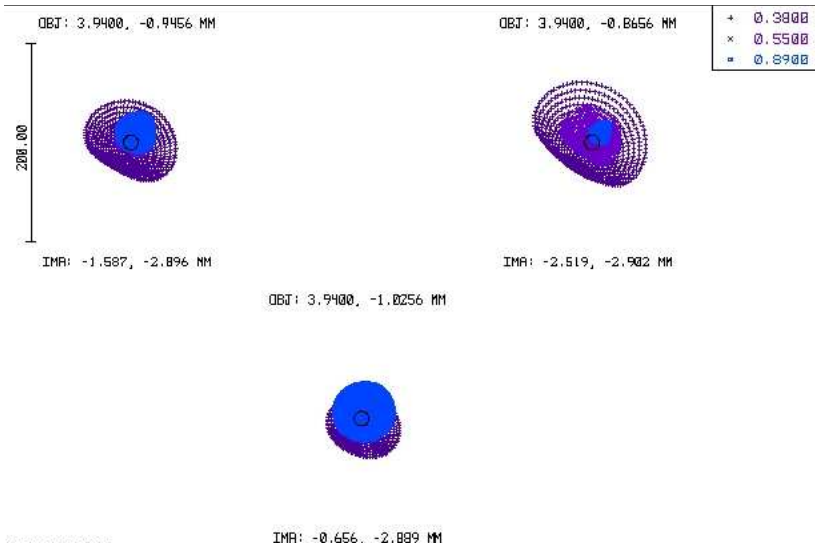

Figure 39: Image quality of the slit transfer optics. The spot diagrams are computed at the location of the slit plate and also include the image slicer optics. The open circle shows the diffraction limit.

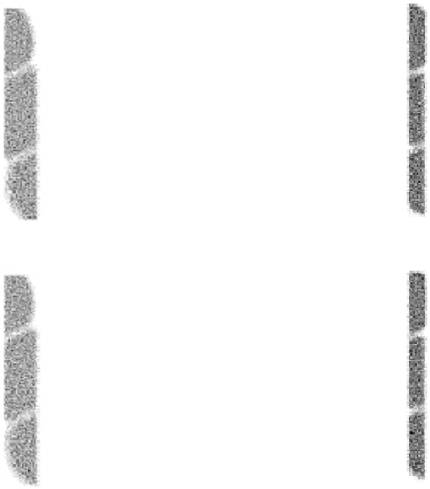

Figure 40: Images of the medium (left) and high (right) resolving power sliced fibres. The image plane is immediately behind the slit plate shown in Figure 21.

5.2.2 Total spectrograph

The image quality of the blue and red arms of the spectrograph is shown in Figure 41 and Figure 42. Wavelengths in five orders from each arm are shown which span the entire detectors for each camera.

A detailed summary of the image quality is shown in Figure 43 and Figure 44. At all wavelengths from $370 < \lambda < 555$nm that are within one half a free spectral range from the blaze wavelength, the blue camera ensures that 80% of the encircled energy is within a box 25μm square. At all these wavelengths over 50% of the energy is within one pixel. The image quality of the red camera is slightly worse. The requirement for 80% of the encircled energy being within 25μm square box is met for wavelengths less than 800nm. The image quality from 800nm to 890nm is degraded to approx 30 – 35μm EE(80) diameter. The greater pixel sampling of the red camera will ensure that the same maximum resolving power can be achieved by both arms.

The vignetting of all optics in the blue and red arms is negligible at all wavelengths within the central free spectral range.

Spot diagrams in each of the medium and high resolving power fibre sliced modes are shown in Figure 45, Figure 47, Figure 49 and Figure 51[2]. The variable effect of the image quality can clearly be seen. Also noticeable is the effect of echelle anamorphic magnification on the slit width. Figure 46, Figure 48, Figure 50 and Figure 52 show the image of a central wavelength in each of the cameras and fibre sliced modes. The image has been rebinned to the 15μm pixel scale of the SALT HRS CCDs. These images clearly show that the optical image quality is adequate to fully resolve the slit images. Detector effects are presently neglected.

[2] Note that slit tilt has not being completely corrected. However, the amount of slit tilt is identical for every slit image and will be corrected during assembly and commissioning.

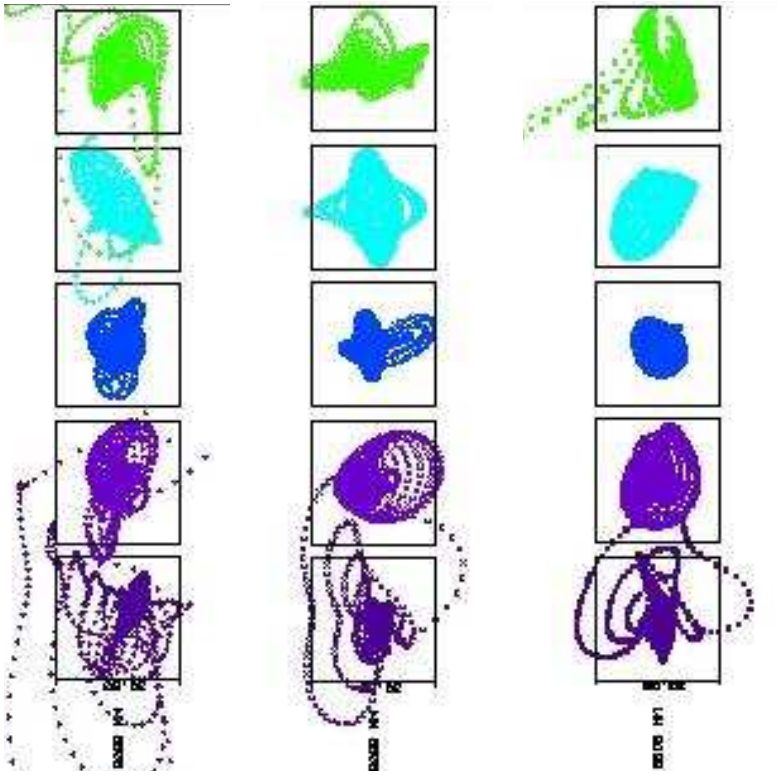

Figure 41: Spot diagrams for the SALT HRS blue arm. Wavelengths from the edges of the free spectral range (left and right columns) and middle of orders 125, 114, 100, 91 and 84 are shown. Each box is 30µm square.

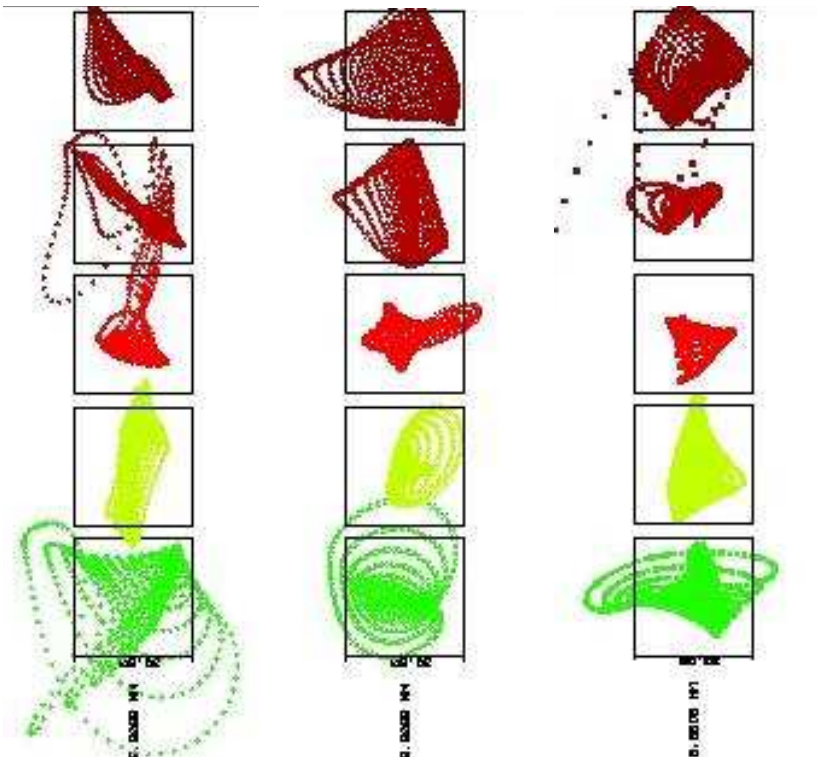

Figure 42: Spot diagrams for the SALT HRS red arm. Wavelengths from the edges of the free spectral range (left and right columns) and middle of orders 85, 77, 64, 57 and 53 are shown. Each box is 30µm square.

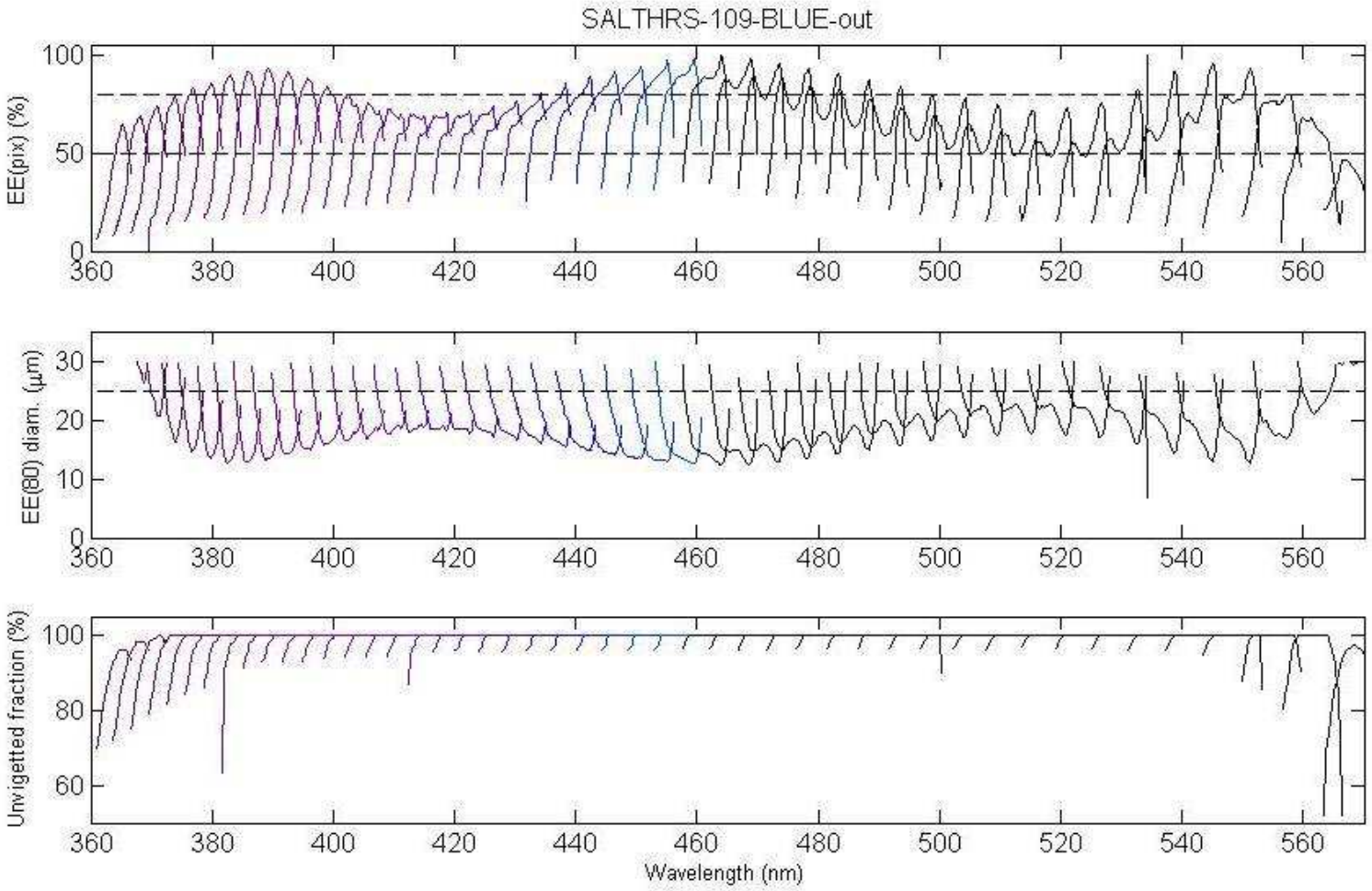

Figure 43: Encirled energy within one 15µm pixel (top), the diameter at 80% encircled energy (middle), and the unvignetted fraction of rays (bottom) for the SALT HRS blue arm. Note that the blue arm wavelength coverage is complete only from 370nm to 555nm.

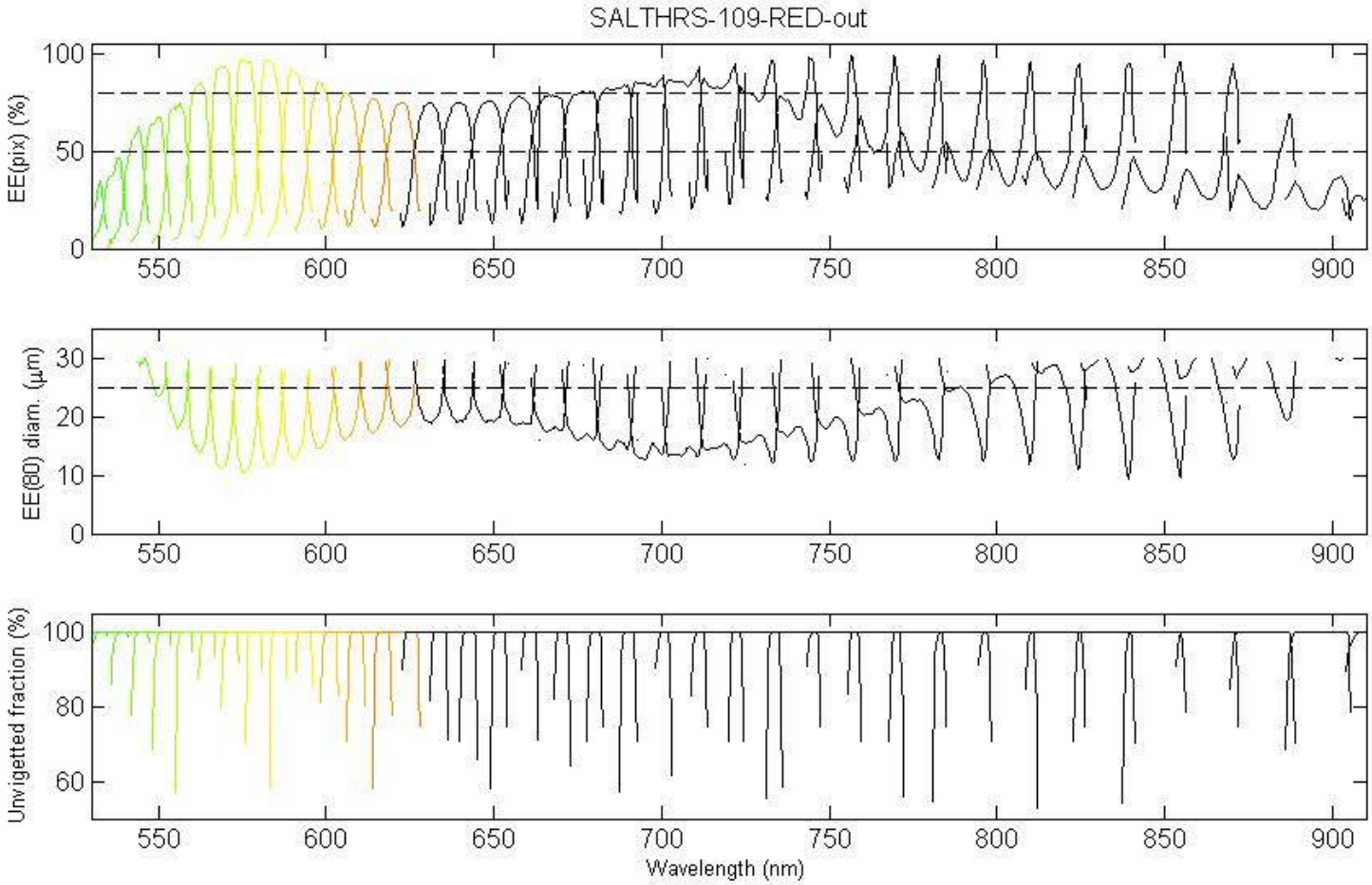

Figure 44: Encirled energy within one 15µm pixel (top), the diameter at 80% encircled energy (middle), and the unvignetted fraction of rays (bottom) for the SALT HRS red arm. Note that the red arm wavelength coverage is complete only from 555nm to 890nm.

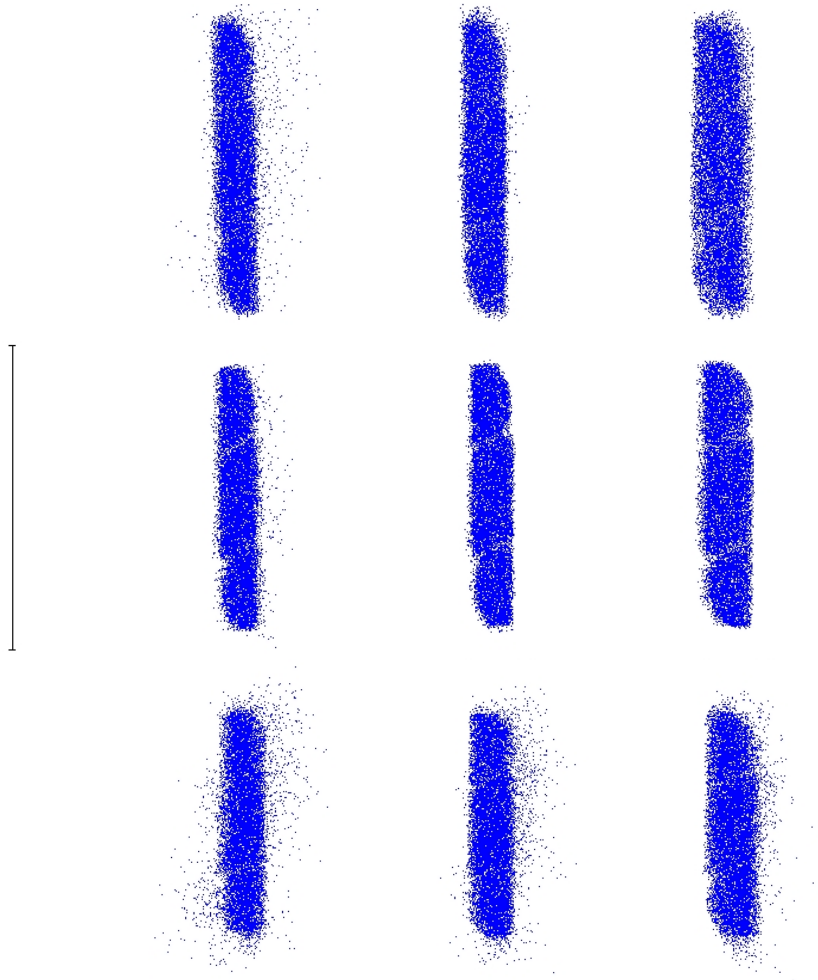

Figure 45: Spot diagrams on the blue camera focal plane in the medium resolution fibre sliced mode. A single sliced fibre is shown for wavelengths spanning a single free spectra range from orders 84 (top), 100 (middle), and 125 (bottom). The scale bar is 0.45mm (30 pixels).

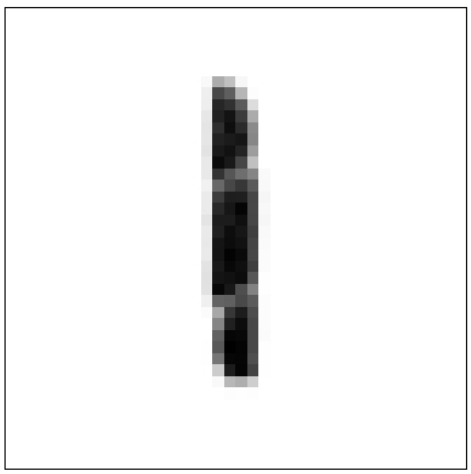

Figure 46: Blue camera image of the central wavelength in the medium resolving power fibre sliced mode. The box is 40 x 40 15µm pixels.

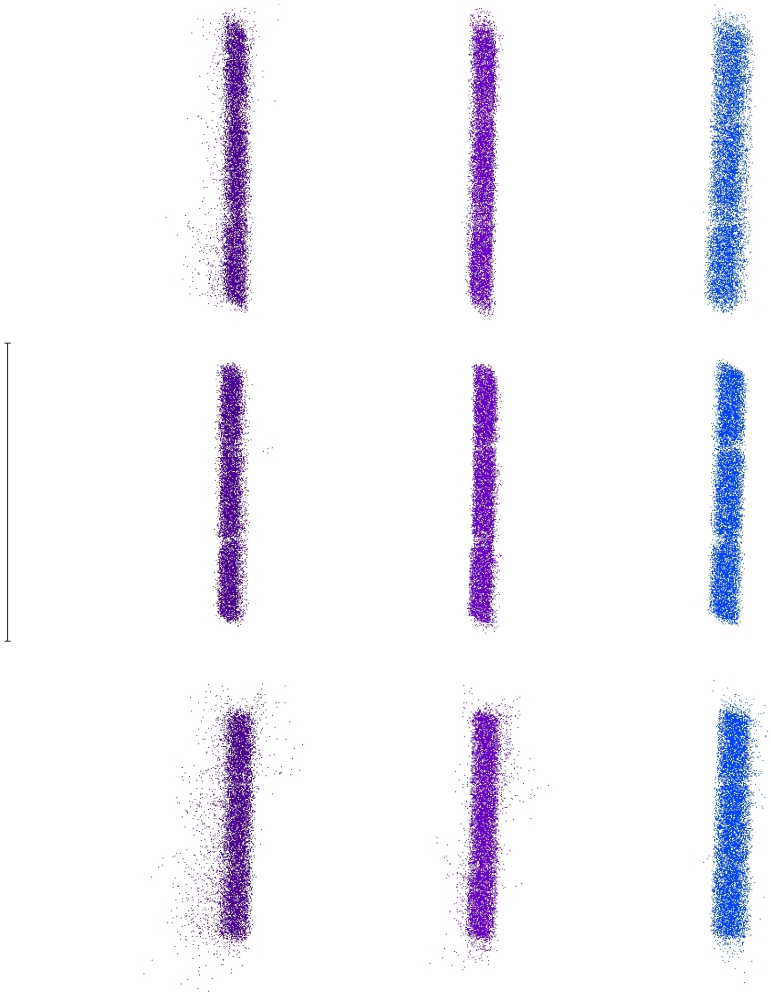

Figure 47: Spot diagrams on the blue camera focal plane in the high resolution fibre sliced mode. A single sliced fibre is shown for wavelengths spanning a single free spectra range from orders 84 (top), 100 (middle), and 125 (bottom). The scale bar is 0.45mm (30 pixels).

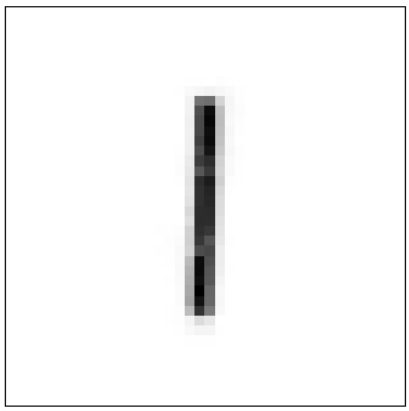

Figure 48: Blue camera image of the central wavelength in the high resolving power fibre sliced mode. The box is 40 x 40 15µm pixels.

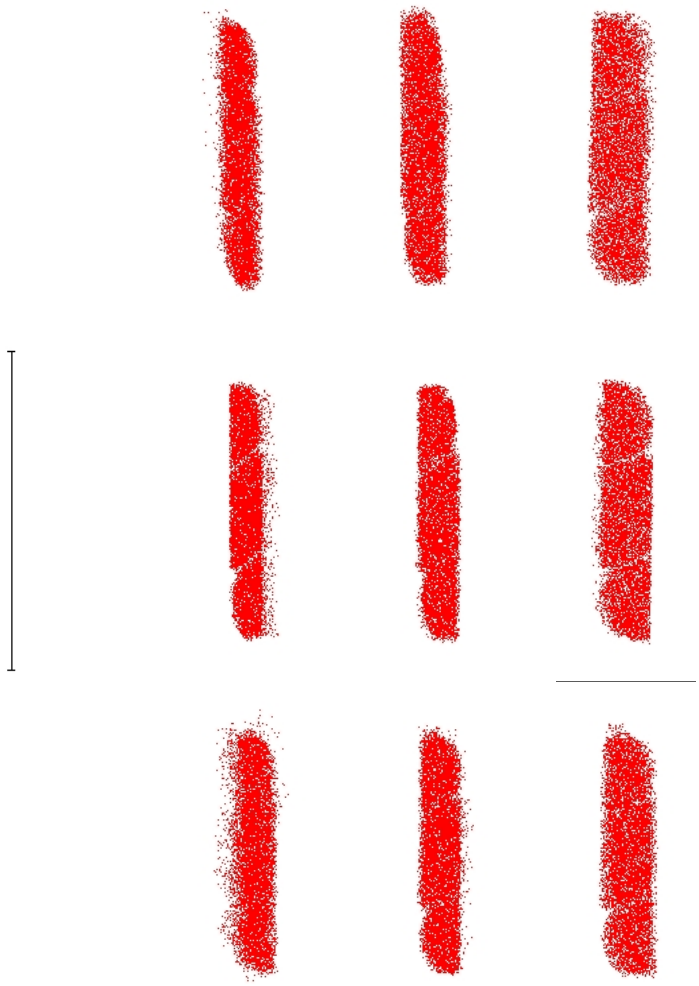

Figure 49: Spot diagrams on the red camera focal plane in the medium resolving power fibre sliced mode. A single sliced fibre is shown for wavelengths spanning a single free spectra range from orders 53 (top), 64 (middle), and 85 (bottom) . The scale bar is 0.60mm (40 pixels).

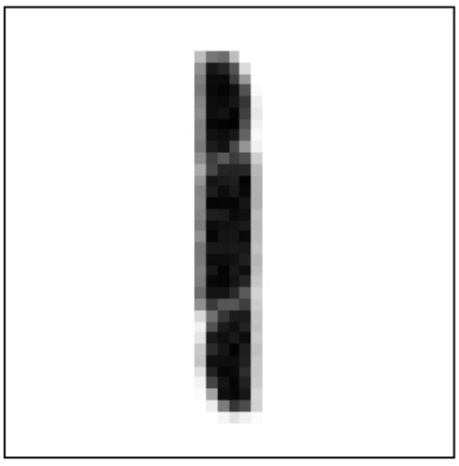

Figure 50: Red camera image of the central wavelength in the medium resolving power fibre sliced mode. The box is 40 x 40 15µm pixels.

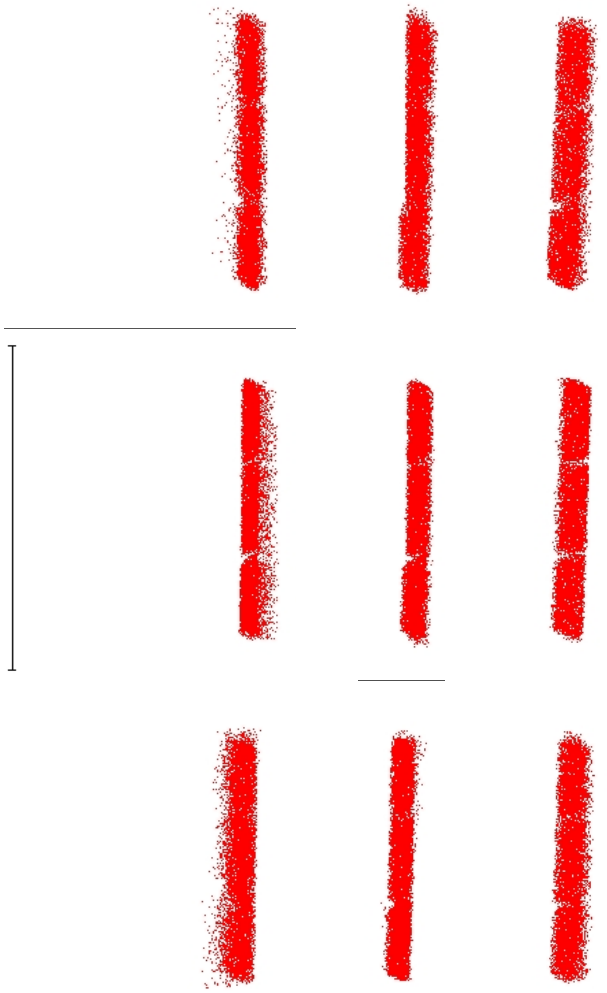

Figure 51: Spot diagrams on the red camera focal plane in the high resolving power fibre sliced mode. A single sliced fibre is shown for wavelengths spanning a single free spectra range from orders 53 (top), 64 (middle), and 85 (bottom). The scale bar is 0.60mm (40 pixels).

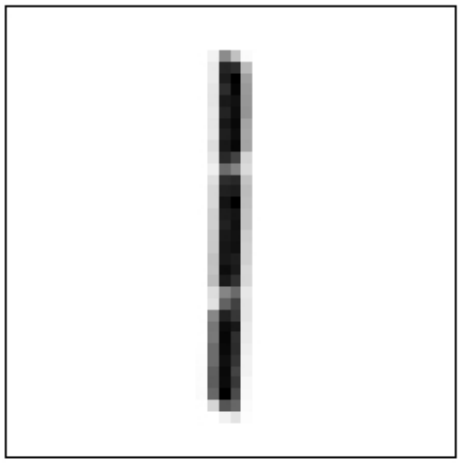

Figure 52: Red camera image of the central wavelength in the high resolving power fibre sliced mode. The box is 40 x 40 15µm pixels.

5.3 Resolving power

The resolving power of SALT HRS is not determined soley by the slit width at the collimator focus. Both the optics and detector will degrade the image of the slit. This will broaden the extracted line spread function (LSF) of any given spectral line leading to a lower resolving power. The predicted resolving power of SALT HRS has been computed using the method outlined by Hans Dekker during the 2004 July PDR and closely follows the method used for validating the performance of UVES[3].

The factors that are assumed to contribute to the degradation of the SALT HRS resolving power include:

- the spectrograph image quality,
- slit image quality and/or defocus,
- CCD flatness and/or defocus,
- CCD opto-electronic PSF ("silicon PSF"), and
- the CCD pixel sampling.

It is assumed that because the number of contributors to the final LSF is large, each contributor can be approximated by a convolution of an initial LSF with degrading LSFs which are all guassian. That is, if the slit limited resolving power is given by R_{sltlim}, then the total resolving power R_{tot} is given by

$$1/R_{tot}^2 = 1/R_{sltlim}^2 + 1/R_{optpsf}^2 + 1/R_{sltpsf}^2 + 1/R_{ffpsf}^2 + 1/R_{eopsf}^2 + 1/R_{smpsf}^2.$$

Each contributor to the total resolving power is described below:

- R_{opt} = the optical PSF. The image quality as predicted by Zemax is used to estimate this quantity. It is assumed that the FWHM of the optical PSF (opt_{psf}) is 1.32 times the RMS image diameter. The PSF is degraded a further 10% to account for camera manufacturing and alignment tolerances.
- R_{slt} = the slit optics PSF. The degradation due to the slit optics will generally be small. A nominal PSF of slt_{psf} = 3.5µm FWHM is assumed.
- R_{ff} = the CCD flatness and/or defocus PSF. A value of ff_{psf} = 7.5µm is assumed.
- R_{eo} = the CCD electro-optical PSF. Again, eo_{psf} = 7.5µm is assumed. This value is quite uncertain in the absence of measured data. The value is perhaps optimistic.
- R_{smp} = the CCD sampling PSF. Simulations show that the 15µm sampling by the CCD pixels is equivalent to a PSF with a FWHM of approx. smp_{psf} = 13µm.

The resolving power R_n resulting from each of the contributions n_{psf} is given by

$$R_n = 2\, R_{max} \times (s_{pix} / n_{psf})$$

[3] http://www.eso.org/observing/dfo/quality/UVES/qc/resolution_qc1.html

where R_{max} is by definition the maximum resolving power of each spectrograph arm assuming Nyquist sampling by pixels which are each s_{pix} = 15μm in size.

Examples of these calculations for a single wavelength in the centre of each of the blue and red cameras follow:

Blue:

```
====
Rmax = 80000, Rslit = 76800,
Contributions to total resolving power:
    Defocus along slit:   fwhm =  3.5 -> R = 680900
    Optical psf (centre): fwhm =  8.9 -> R = 240400
    CCD flatness/defocus: fwhm =  7.5 -> R = 317800
    CCD "silicon psf":    fwhm =  7.5 -> R = 317800
    CCD sampling:         fwhm = 13.1 -> R = 182600
-> Rtot = 64700.
```

```
Red:
====
Rmax = 100000, Rslit = 76800
Contributions to total resolving power:
    Defocus along slit:   fwhm =  3.5 -> R = 851200
    Optical psf (centre): fwhm =  9.6 -> R = 277800
    CCD flatness/defocus: fwhm =  7.5 -> R = 397200
    CCD "silicon psf":    fwhm =  7.5 -> R = 397200
    CCD sampling:         fwhm = 13.1 -> R = 228300
-> Rtot = 68100.
```

It is important to note that the echelle anamorphic magnification will affect these effective resolving powers. In the blue orders the anamorphic magnification *r* varies as $0.82 < r < 1.22$ from one side of the free spectral range to the other. In the red arm, the spread is $0.76 < r < 1.41$. The result is that the sampling of each resolution element will vary significantly from one side of the order to the other. Calculations of the resolving power in each of the fibre sliced modes for all wavelengths are shown in Figure 53 and Figure 54.

From Figure 53 it can be seen that the target resolving power is achieved at all essentially all wavelengths. This is certainly true for all wavelengths within one half of a free spectral range of the blaze wavelength. The resolving power at the order centre, where effects of echelle anamorphism are minimized, and where the image quality is best, are within 5 or 10% of the slit limited resolving power.

In Figure Figure 54 it is seen that all blaze wavelengths from 370nm to 890nm achieve the target resolving power. A significant fraction of wavelengths have resolving powers less than the target. This is primarily the result of the resolution undersampling caused by the large variation in anamorphic magnification. It will only affect wavelengths on one half of each spectral format.

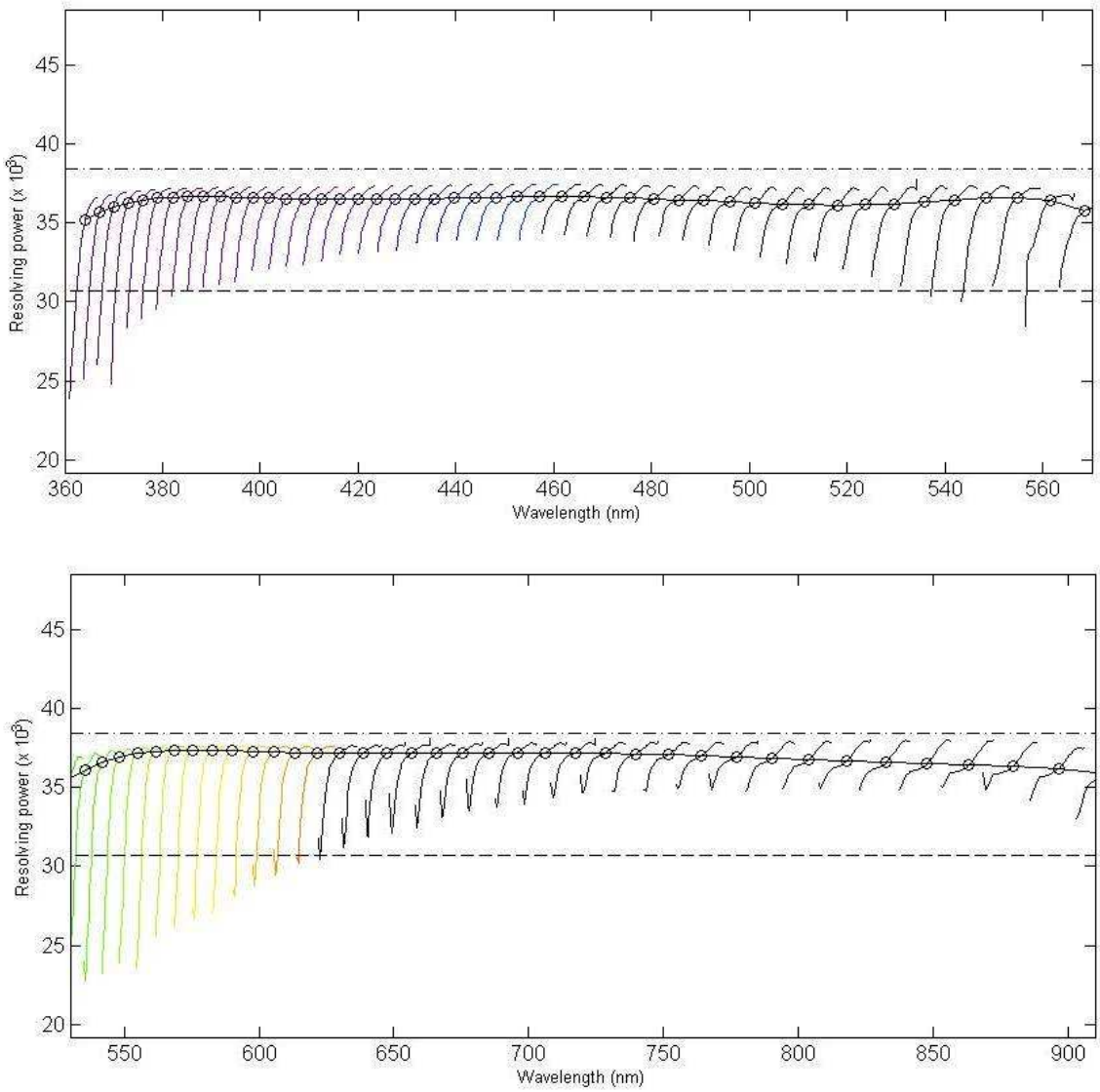

Figure 53: The resolving power of SALT HRS in the medium resolving power fibre sliced mode. The top panel shows the blue arm while the bottom shows the red arm. Each orders covers more than a single free spectral range. The dot-dashed line is the slit limited resolving power and the dashed line is the target resolving power. Open circles show the resolving power in the order centre where there is no échelle anamorphism.

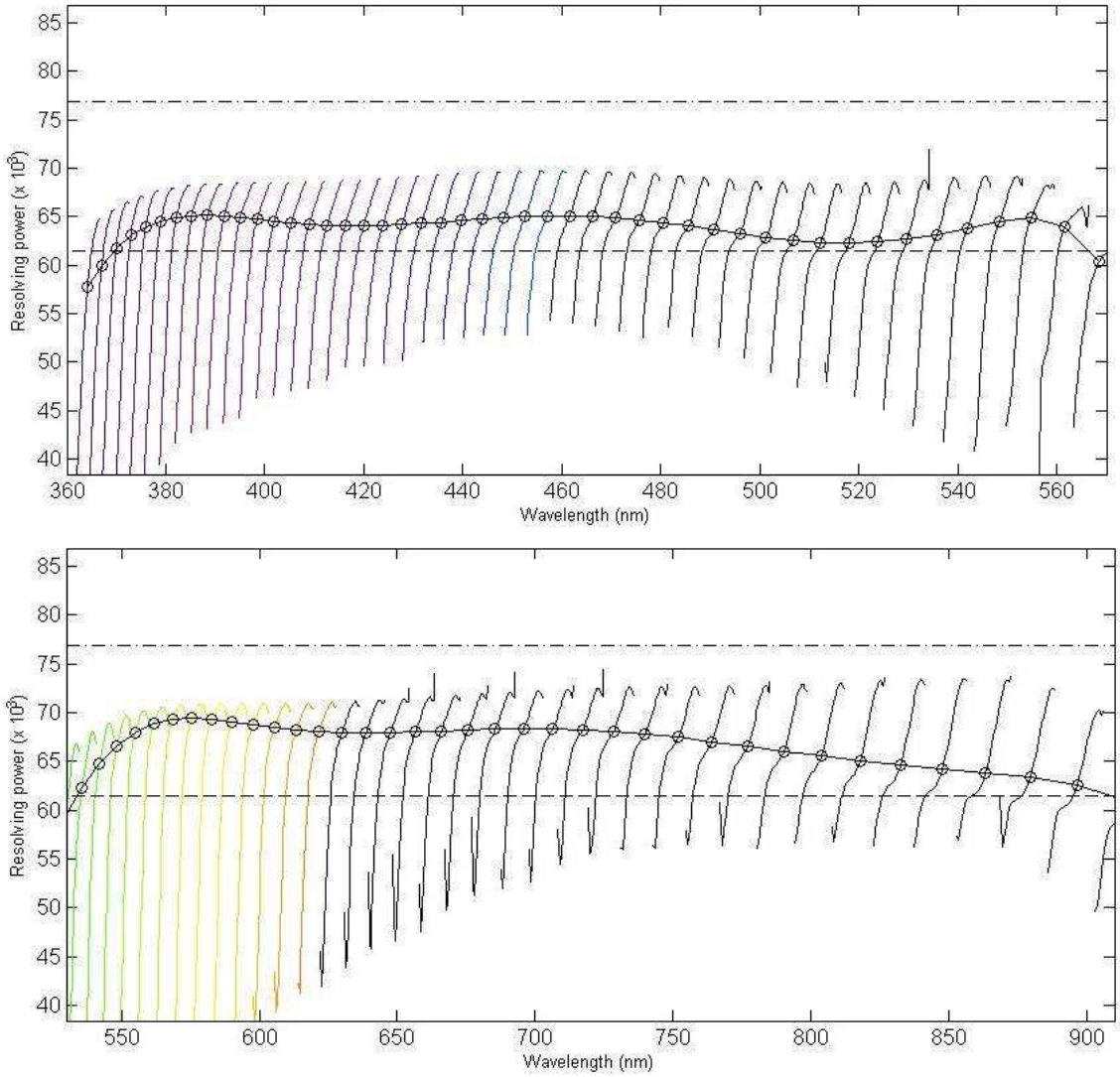

Figure 54: The resolving power of SALT HRS in the high resolving power fibre sliced mode. The top panel shows the blue arm while the bottom shows the red arm. Each orders covers more than a single free spectral range. The dot-dashed line is the slit limited resolving power and the dashed line is the target resolving power. Open circles show the resolving power in the order centre where there is no échelle anamorphism.

5.4 Thermal analysis

In order to assess the thermal stability requirements of SALT HRS a thermal analysis was performed using Zemax. All non-glass spaces were assumed to have a coefficient of thermal expansion equal to that of either aluminium (25 x 10-6/°C) or steel (12 x 10-6/°C). The coefficient of thermal expansion of glass components was taken from the Zemax catalogue and checked against manufacturers data where possible. A total temperature range from 5°C to 35°C was investigated.

The effect that a temperature change has on image quality is assessed in Figure 55 in terms of the spectrograph's merit function. It can be seen that a temperature change has a large effect on the image quality if the spectrograph remains unfocused. However, if at any given temperature the spectrograph is refocused (using the blue or red pupil mirrors) the image quality is degraded by less than 5% from the image quality at the nominal design temperature (20°C).

The focus distance for each pupil mirror as a function of temperature is shown in Figure 56. Given that the focus position is approximated very well by a linear fit it would be possible to automatically focus the pupil mirrors as the temperature changes. However, this will not be necessary if the operating temperature of SALT HRS is stable to within (±0.5°C) during one day.

It is found that a small temperature change (±0.5°C) has a negligible effect on the line position in the direction of echelle dispersion at any given temperature (assuming the spectrograph is focused). The orders will migrate in the direction of cross-dispersion by less than 2μm/°C (at a fixed focus). The shift is 4μm/°C across the total range of temperatures investigated.

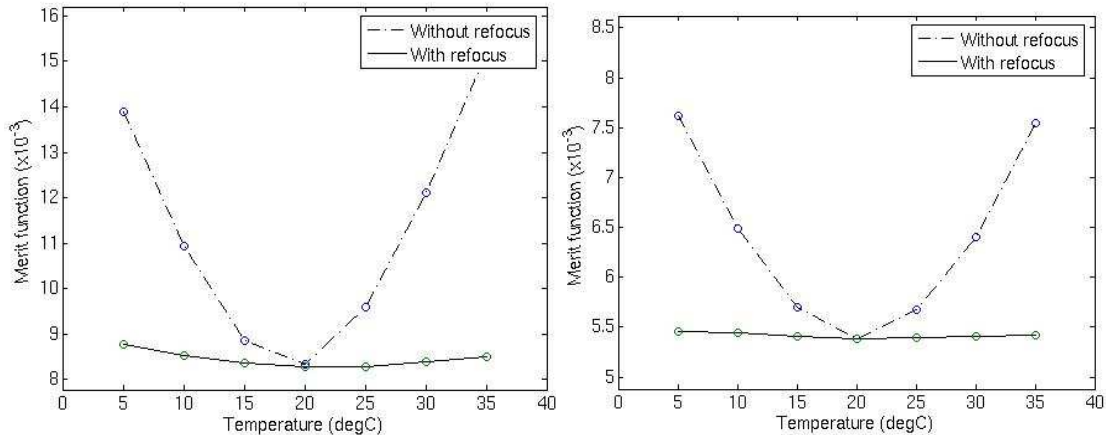

Figure 55: Merit functions for the blue (left) and red (right) arms of SALT HRS as a function of temperature. The dashed line shows the merit function without refocusing the pupil mirror while the solid line shows the merit function after refocus.

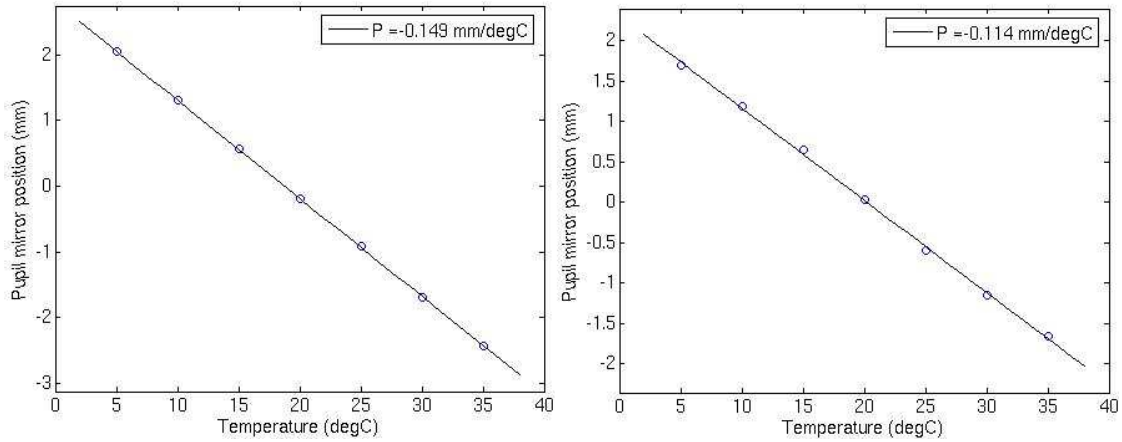

Figure 56: Pupil mirror focus positions as a function of temperature for the blue (left) and red (right) arms of SALT HRS.

5.5 Efficiencies

5.5.1 SALT

The reflectance of each SALT mirror has been measured. The SAC reflectivities are from witness samples made at the time of coating while the primary mirror (aluminium) reflectivity is that of a standard coating. The image quality is assumed to be *EE(80)* = 2.15″. The absorption of due to the two elements of the atmospheric dispersion corrector have also been estimated. It is assumed that the mirrors are freshly installed.

5.5.2 FIF and fibres

It is assumed that Polymicro FBP fibres or an equivalent which uses Hearaus STU performs will be used. The fibres are assumed to have overcoated micro-lenses (or flat windows) at both the input and output. The geometrical throughput of all fibres due to the finite seeing disk has been calculated assuming 1.12 arcsec FWHM images.

5.5.3 Image slicers and intermediate transfer optics.

Geometrical throughputs of ~80% and ~90% are used for the medium and high resolution image slicers respectively. It is assumed that the throughput of the image slicers is 95% of this value due to scattering and absorption. The efficiencies of the image slicers are **TBC** upon construction.

It is assumed that all transfer optics and windows have efficient multi-layer broad-band coatings.

5.5.4 Mirrors

The coatings specified for each of the mirrors are:

- M_1 (collimator and first pupil mirror) – UV enhanced silver,
- M_2 (blue pupil mirror) – enhanced aluminium, and
- M_3 (red pupil mirror) – enhanced silver.

It may be possible to enhance the efficiency of SALT HRS by using alternative mirror coatings. In particular, the use of a multi-layer overcoated coating should be investigated for mirrors that are shared by both blue and red arms. The small collimator fold mirror is assumed to have such a coating.

5.5.5 VPH gratings

Data supplied by Wasatch is used to compute the VPH grating efficiencies. The data is "corrected" to allow for the use of multi-layer coatings on the VPH lenses.

5.5.6 Cameras

Standard absorption data are used for each of the camera lens elements. A generic broad-band coating has been specified on each element apart from the field-flattening lens which is single-layer MgF_2.

5.5.7 CCDs

The blue arm CCD is assumed to be an E2V 44-82 with a "StdSi astroBB" coating. The red arm CCD is a Fairchild 486 which has their broadband overcoat applied.

5.5.8 Results

The computed efficiencies of SALT HRS R4 are given in the following tables. The spectrograph efficiencies (SPC) include everything except the telescope (TEL) and slit optics (SLT). The slit optics include fibres and where appropriate both slit fore-optics and image slicers. The other items are the collimator (COL), which includes overfilling due to FRD, the échelle grating (ECH), the cross-dispersers (XDP), the camera (CAM), and the CCD. The camera includes the white pupil mirrors **and** dichroic.

Table 7: Detailed efficiencies of the SALT HRS R4 blue arm at the lowest resolving power.

Lam. λ	Ord. M	Component by component efficiencies (the slit mode is "Fixed object" at *R* = 16,000)							Totals		
		TEL	SLT	COL	ECH	XDP	CAM	CCD	SPC	SPC + SLT	SPC + SLT + TEL
379.3	123	0.601	0.458	0.749	0.569	0.744	0.538	0.674	0.115	0.053	0.032
481.0	97	0.623	0.684	0.912	0.623	0.885	0.777	0.803	0.314	0.215	0.134
542.6	86	0.616	0.724	0.910	0.607	0.668	0.731	0.795	0.214	0.155	0.096

Table 8: Detailed efficiencies of the SALT HRS R4 red arm at the lowest resolving power.

Lam λ	Ord M	Component by component efficiciences (the slit mode is "Fixed object" at *R* = 16,000)							Totals		
		TEL	SLT	COL	ECH	XDP	CAM	CCD	SPC	SPC + SLT	SPC + SLT + TEL
562.2	83	0.619	0.733	0.908	0.601	0.856	0.817	0.832	0.318	0.233	0.144
648.1	72	0.596	0.751	0.901	0.588	0.945	0.824	0.942	0.389	0.292	0.174
804.5	58	0.588	0.782	0.896	0.582	0.533	0.811	0.903	0.203	0.159	0.094

Table 9: Summary of efficiencies of the SALT HRS R4 blue arm at all resolving powers and modes at a wavelength of 480 nm.

Fibre mode	Resolving Power (λ/δλ)	Transmission		
		SPC	SPC + SLT	SPC + SLT + TEL
Low	16,000	31.4%	21.5%	13.4%
Medium	~37,000	31.4%	15.1%	9.4%
High	~65,000	31.4%	9.6%	6.0%

Table 10: Summary of efficiencies of the SALT HRS R4 red arm at all resolving powers and modes at a wavelength of 650 nm.

Fibre mode	Resolving Power (λ/δλ)	Transmission		
		SPC	SPC + SLT	SPC + SLT + TEL
Low	16,000	38.9%	29.2%	17.4%
Medium	~37,000	38.9%	20.3%	12.1%
High	~65,000	38.9%	12.9%	7.7%

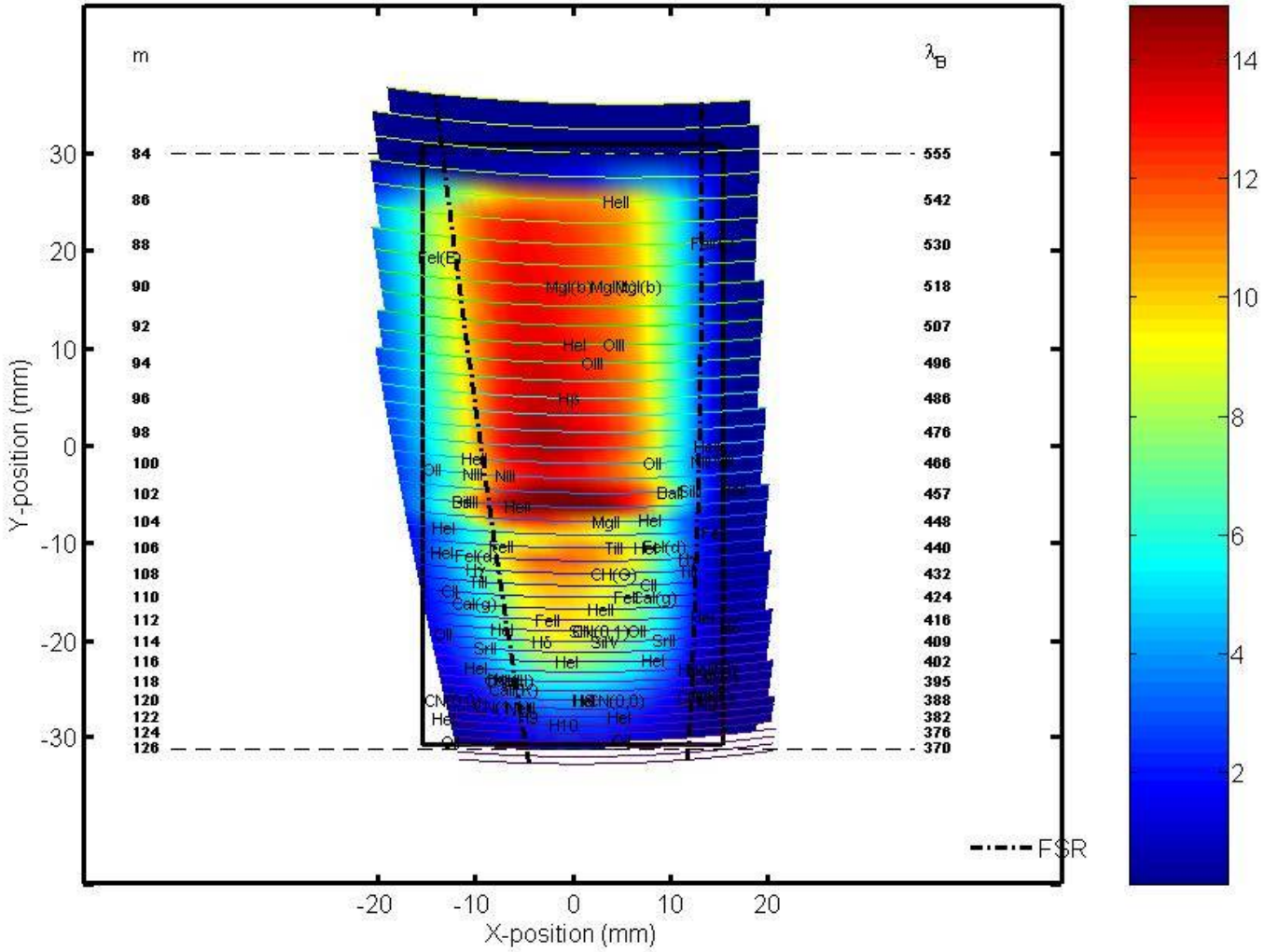

Figure 57: The efficiency of the blue spectrograph arm at all wavelengths in the low resolving power mode. All optics from the telescope to the CCD are included.

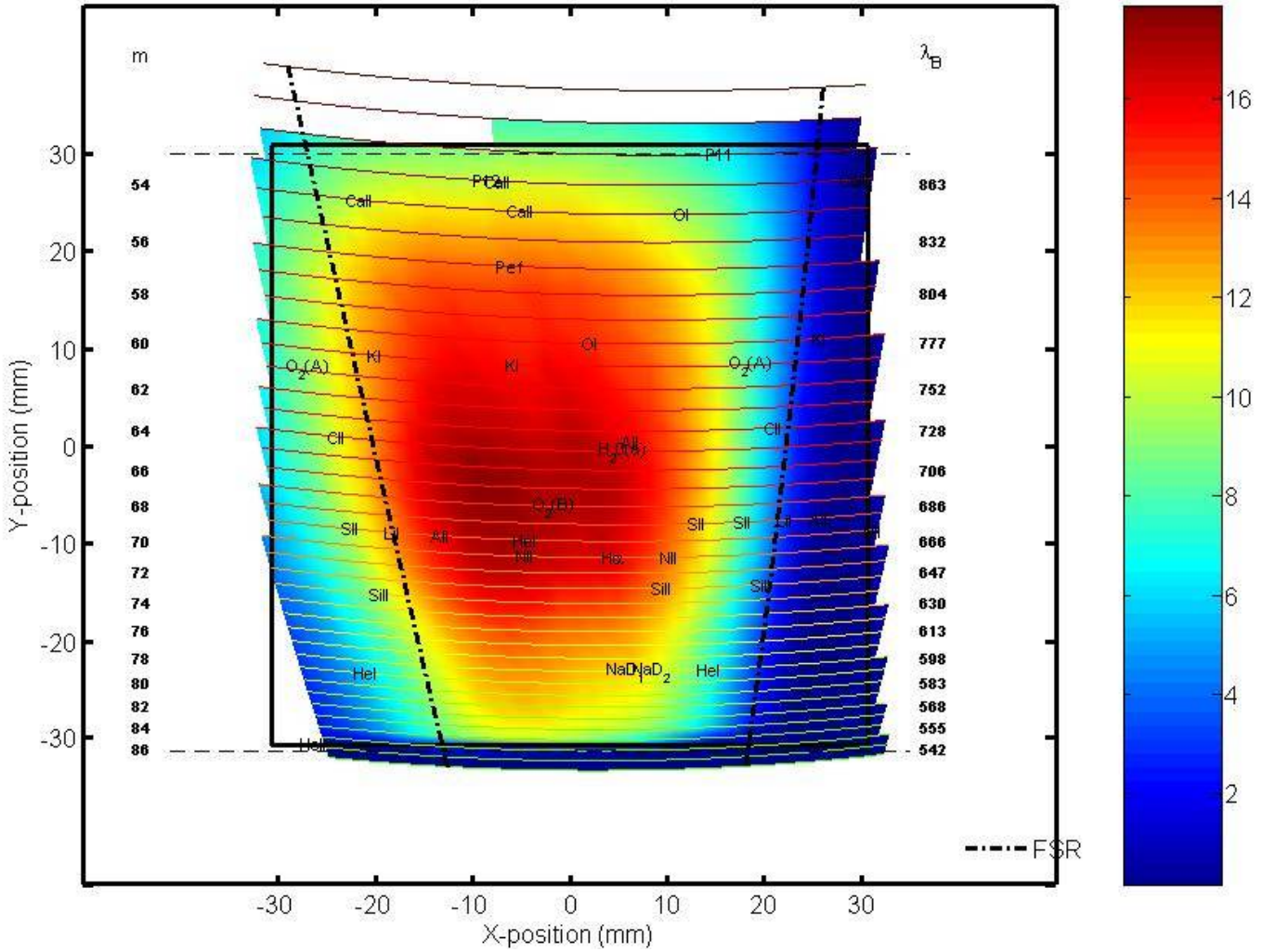

Figure 58: The efficiency of the blue spectrograph arm at all wavelengths in the low resolving power mode. All optics from the telescope to the CCD are included.

5.5.9 Signal to noise predictions

Using the above efficiency calculations the signal to noise expected for a range of observing conditions has been computed. The following calculations assume a G dwarf star and a telescope airmass of 1.3. The moon is assumed to be quarter phase. The calculated signal to noise ratios (S/N) are for each extracted half-resolution element (to allow correct for Nyquist sampling). The results for the blue and red arms are shown in Figure 59 and Figure 60.

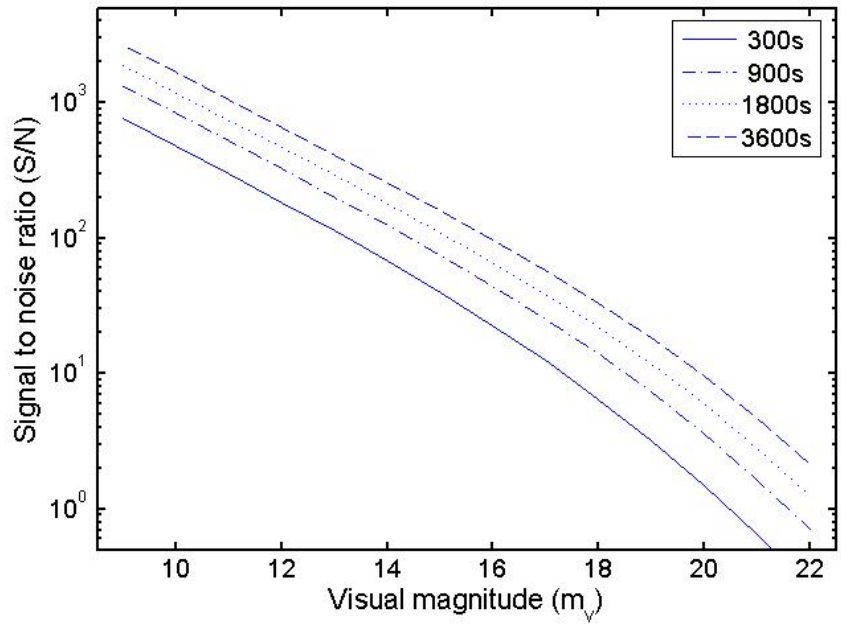

Figure 59: Signal to noise predictions for the SALT HRS blue arm at 480nm.

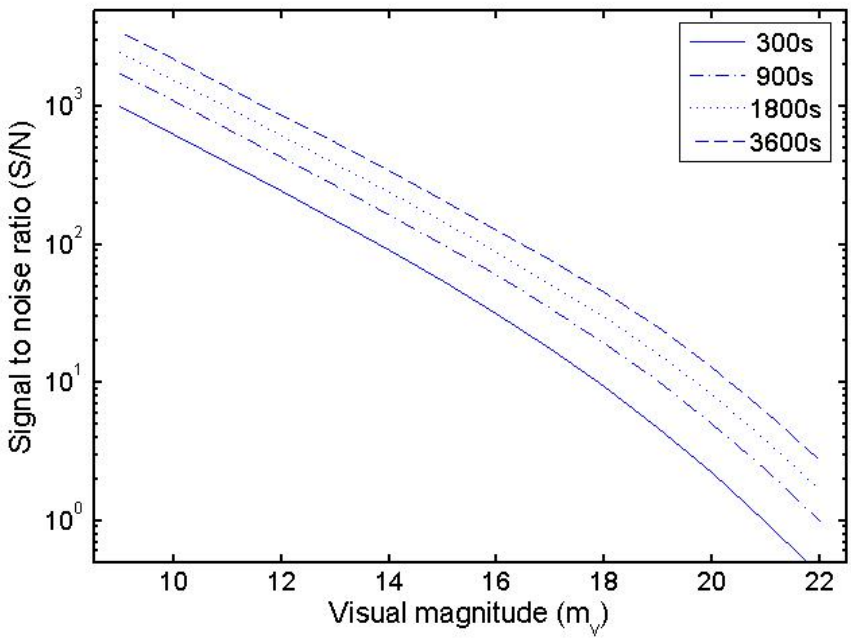

Figure 60: Signal to noise predictions for the SALT HRS red arm at 650nm.

6 Optical upgrade options

The optical design has provision for various upgrade options. All of the following involve changes only to the fibre feed optics:

1) Nod and shuffle at higher resolving powers. These modes are described in the PDR version of this document.

2) Iodine cell. An iodine cell may be inserted in the intermediate injection light path at the same location as the slit viewing optics fold mirror. Space has been provided in the fibre interchange mechanism for this.

3) Fibre double-scrambling.

4) Simultaneous thorium argon.

5) Other fibre feed options. E.g.:
   - Higher resolving power direct injection fibres.
   - Externally disperser interferometer.

Option 1) may be required for high accuracy sky substraction at high resolving powers. It requires only that a new set of fibre image slicers be specified.

Any or all of options 2), 3) and 4) are required for enhanced radial velocity stability

Option 2) will require that the iodine cell be mounted in a cell with an optic to correct for the change in path length.

Option 3) requires an alternative fibre mode which involves a junction with a double-scrambler and may be implemented without any alternation to the present optics. The concept of fibre-double scrambing is discussed in Brown 1990.

Option 4) requires a pair of dedicated fibres and/or image slicers for each resolving power. One fibre from each pair must terminate at a laboratory thorium argon source. This source must provide control for thorium lamp intensity. The laboratory source may also be required to emulate the SALT moving pupil. Alternatively, this mode could be combined with Option 3) (double-scrambling).

Improvements in telescope image quality may allow higher resolving power to be achieved with smaller fibre without a loss in throughput. This fibres would be placed at the direct injection location.

Discussions of the potential of using an externally dispersed interferometer EDI to boost resolving power may be found in Erskine and Edelstein 2004. An EDI has the potential to be placed near the location of the slit viewing camera optics.

7 References

Brown, T. "High precision Doppler measurements via echelle spectroscopy" in CCDs in astronomy; Proceedings of the Conference, Tucson, AZ, Sept. 6-8, 1989
http://cdsads.u-strasbg.fr/cgi-bin/nph-bib_query?bibcode=1990ASPC....8..335B

Buckley, D., Cottrell, P., Nordsieck, K., O'Donoghue, D., and Williams, T. "The First-Generation Instruments for the Southern African Large Telescope", Proceedings of Large Telescopes and their Instrument, SPIE, 2004 (in press).
http://cdsads.u-strasbg.fr/cgi-bin/nph-bib_query?bibcode=2004SPIE.5492...60B

Buckley, D. "SALT Calibrations", a presentation to the SSWG, May 2004.

Erskine, David J. and Edelstein, Jerry, "Interferometric resolution boosting for spectrographs", UV and Gamma-Ray Space Telescope Systems. Edited by Hasinger, Günther; Turner, Martin J. L. Proceedings of the SPIE, Volume 5492, pp. 190-199 (2004).
http://cdsads.u-strasbg.fr/cgi-bin/nph-bib_query?bibcode=2004SPIE.5492..190E